ARTICLE

One Endothelium-Targeted Combined Nucleic Acid Delivery System for Myocardial Infarction Therapy

Yihui Shao,[#] Chen Xu,[#] Shuolin Zhu, Jianing Wu, Canghao Sun, Shan Huang, Guoqi Li, Weijie Yang, Ting Zhang, Xin-Liang Ma, Jie Du, Ping Li, Fu-Jian Xu,* and Yulin Li*

Cite This: https://doi.org/10.1021/acsnano.3c11661 — Read Online

| ACCESS | 📊 Metrics & More | 📖 Article Recommendations | 🆘 Supporting Information |

ABSTRACT: Acute myocardial infarction (MI) and ischemic heart disease are the leading causes of heart failure and mortality. Currently, research on MI treatment is focused on angiogenic and anti-inflammatory therapies. Although endothelial cells (ECs) are critical for triggering inflammation and angiogenesis, no approach has targeted them for the treatment of MI. In this study, we proposed a nonviral combined nucleic acid delivery system consisting of an EC-specific polycation (CRPPR-grafted ethanolamine-modified poly(glycidyl methacrylate), CPC) that can efficiently codeliver siR-ICAM1 and pCXCL12 for the treatment of MI. Animals treated with the combination therapy exhibited better cardiac function than those treated with each nucleic acid alone. In particular, the combination therapy of CPC/siR-ICAM1 and CPC/pCXCL12 significantly improved cardiac systolic function, anti-inflammatory responses, and angiogenesis compared to the control group. In conclusion, CPC-based combined gene delivery systems show impressive performance in the treatment of MI and provide a programmed strategy for the development of codelivery systems for various EC-related diseases.

KEYWORDS: *gene therapy, polycationic delivery system, myocardial infarction, combined therapeutic approach, cardiac targeting*
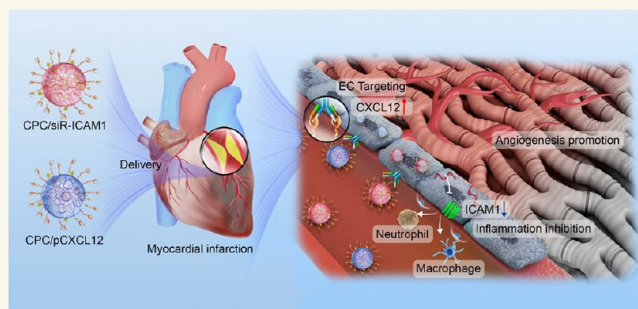
INTRODUCTION

Acute myocardial infarction (MI) due to coronary artery occlusion is the leading cause of morbidity and mortality worldwide.[1,2] Cardiac dysfunction occurs due to progressive cell death in under-perfused areas caused by myocardial ischemia.[3,4] Currently available treatments for revascularization include coronary artery bypass grafting and percutaneous coronary intervention (PCI); however, some patients are ineligible for these therapies, necessitating the development of effective approaches.[5,6]

Previous studies have identified two key pathological processes involved in cardiac repair following MI: the acute inflammatory phase, characterized by the adhesion of inflammatory cells to and invasion of the heart tissue and myocardium, and the subsequent reparative phase.[7,8] Imbalances between tissue damage and repair lead to adverse cardiac remodeling and dysfunction.[9,10] Endothelial cells (ECs) could play a decisive role in MI, as they are more susceptible to MI than cardiomyocytes (CM).[11] During the acute inflammatory phase, ECs express abundant adhesion molecules, facilitating the firm adhesion and migration of circulating leukocytes

through the vessel wall into the myocardium.[12,13] During the repair phase, ECs proliferate and migrate to promote angiogenesis and facilitate cardiac repair.[14] Therefore, interventions targeting ECs to inhibit early inflammation and promote repair capacity hold potential for treating MI. ICAM-1, the member of the superfamily of cell adhesion molecules produced by ECs, is required for the migration of leukocytes through the endothelium and into the heart, where they release toxic metabolites that damage the latter. Inhibition of ICAM-1 decreases the adhesion of leukocytes to ECs.[11,15] Furthermore, several previous studies have shown that CXCL12, a C-X-C chemokine, causes migration of endothelial progenitor cells (EPCs) to areas of ischemia by interacting with the G-protein-coupled receptor CXCR4.[16,17] In a more recent study,
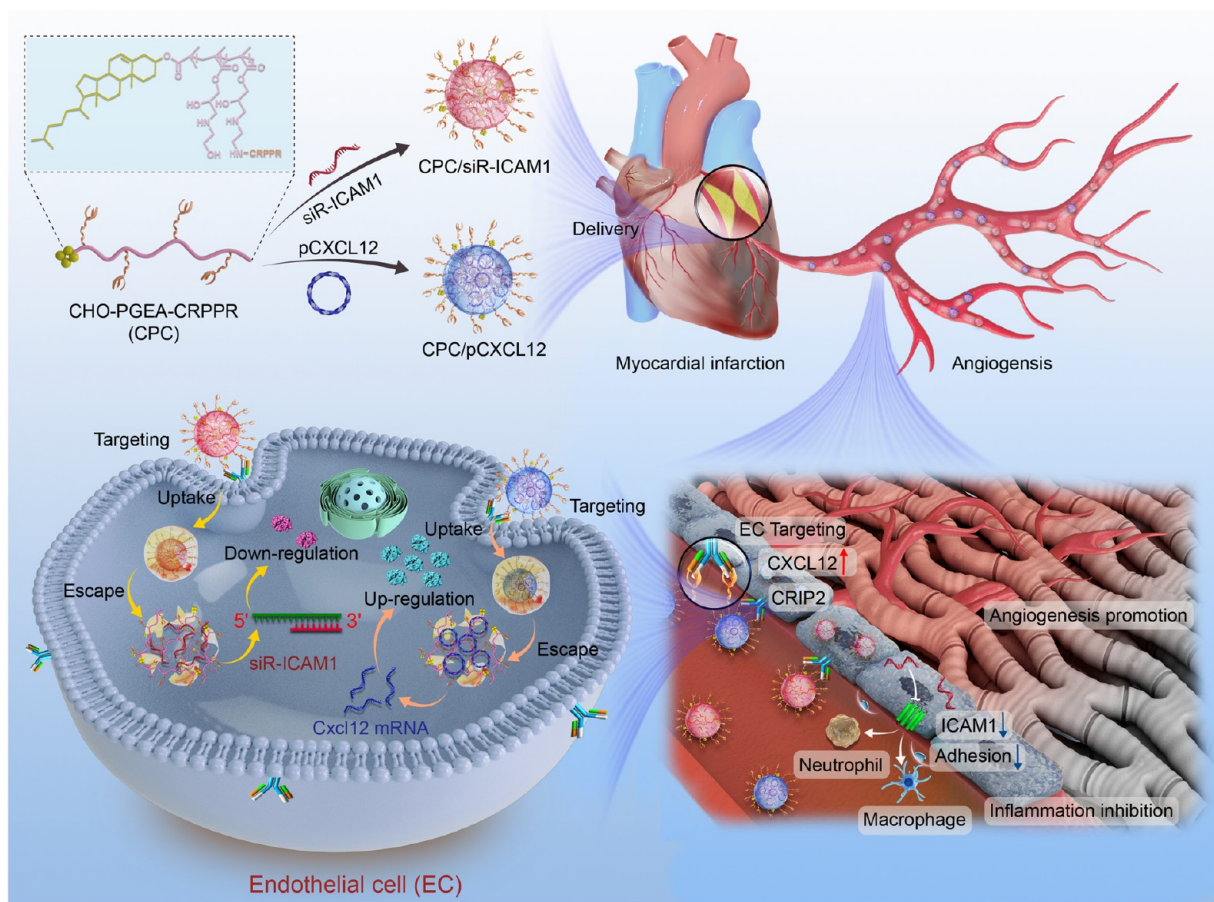
Figure 1. Schematic illustration of the construction of CPC/siR-ICAM1 and CPC/pCXCL12 complexes and cardiac endothelium-targeted combination therapy for myocardial infarction.

CXCL12 was reported to induce ECs migration from arteries along preexisting capillaries and reaccumulate in collateral arteries.[18] However, there are currently no therapies specifically targeting ECs during MI. Therefore, a promising approach involves targeting cardiac ECs using a combination of ICAM1 and CXCL12.

Nanocarriers have become an effective delivery system to reduce the off-target effect and increase the cycle time of gene therapy drugs. Polycations, one of the most important types of nonviral vectors, are positively charged and play a crucial role in gene therapy. Through electrostatic interactions, they can compress negatively charged nucleic acids into nanocomplexes. This condensation not only protects the genetic material from degradation but also facilitates its uptake into cells. A series of polycation-based vectors have been developed to effectively deliver various nucleic acids in cardiovascular diseases.[19−21] Specifically, cholesterol (CHO)-terminated ethanolamine-aminated poly(glycidyl methacrylate) (CHO-PGEA, CPE) nanoparticles exhibit high transfection efficiency for small RNA in the heart.[22]

In this study, we developed a cardiac endothelium-targeted delivery system by administering a combination of ICAM1 and CXCL12 (Figure 1). The aim was to inhibit inflammatory cell infiltration, particularly in the acute inflammatory phase, and promote angiogenesis in the repair phase of MI to achieve therapeutic effects.

RESULTS

Preparation and Characterization of CHO-PGEA-CRPPR. We aimed to modify CPE as an effective carrier, specifically targeting cardiac ECs. *In vitro* screening has revealed that short linear peptide CRPPR binds specifically to the cardiac endothelium.[23] We investigated whether it could efficiently target the cardiac endothelium for specific delivery. Therefore, CRPPR was conjugated to CPE (CHO-PGEA/ ethyl diamine (ED)-CRPPR, CPC) to further enhance its cardiac-targeting ability. A CPE with a molecular weight of approximately 9.7×10^3 g mol^{-1} was selected to prepare CPE and CPC. Herein, the complexation of cationic polymers grafted with 1, 6, and 12 peptides (CRPPR) and plasmids was simulated. The red dots on the simulation plot represent the sulfur elements of cysteine in the targeting peptides (Figure S1A), while the radial distance distribution of these elements from the complexed DNA surface was calculated in Figure S1B. Based on the results, we concluded that excessive grafted peptide cannot contribute to a high targeting ability. For CRPPR conjugation, CHO-PGEA/ED, a different PGMA derivative with a primary amine species, was created. The epoxy groups in CHO-PGEA were combined with excess ethanol amine (EA) and ED to form CHO-PGEA/ED; the molar ratio of EA to ED was approximately 9:1 (Figure S2). To introduce CRPPR and produce CPC, an amination reaction was carried out using the primary amino groups of CHO-PGEA/ED. The typical ^{1}H NMR spectra of CHO-Br, CHO-PGMA, CHO-PGEA/ED and CPC are shown in Figure
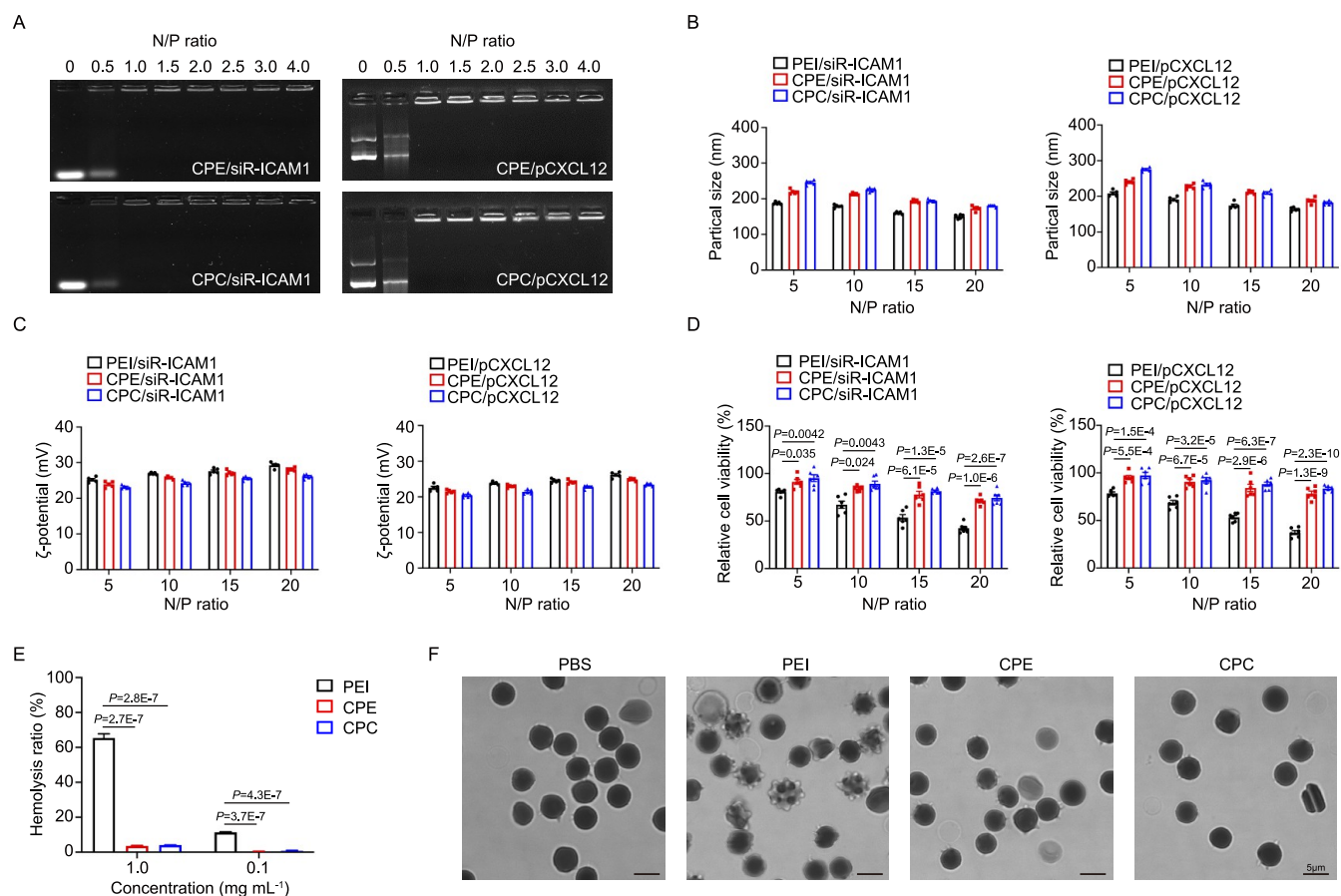
Figure 2. Preparation and characterization of CHO-PGEA/ED-CRPPR. (A) Electrophoretic mobility retardation assay of polycation/siR-ICAM1 and polycation/pCXCL12 complexes at various N/P ratios. **(B)** Particle size of the polycation/siR-ICAM1 and polycation/pCXCL12 complexes at various N/P ratios ($n = 5$ biologically independent samples per group). **(C)** Potentials of polycation/siR-ICAM1 and polycation/pCXCL12 complexes at various N/P ratios ($n = 5$ biologically independent samples per group). **(D)** Cytotoxicity of the polycation/siR-ICAM1 and polycation/pCXCL12 complexes at different N/P ratios ($n = 6$ biologically independent samples per group). **(E)** Hemolysis ratio of RBCs treated with PEI, CPE, and CPC at a concentration of 0.1 and 1 mg mL^{-1} ($n = 3$ biologically independent samples per group). **(F)** Images of red blood cells (RBCs) treated with PEI, CPE and CPC at a concentration of 1 mg mL^{-1}, with PBS serving as a control. Scale bars, 5 μm. Statistical significance was evaluated using the Kruskal−Wallis test followed by Dunn's multiple comparison test (D-siR-ICAM1-10) and one-way ANOVA followed by Tukey's multiple comparison test (D-siR-ICAM1-5, -15, -20, -pCXCL12, and E). All data are presented as mean ± SEM.

S2 and analyzed in detail, demonstrating the effective synthesis of these materials. The reaction efficiency of the peptides was evaluated by using rhodamine B by fluorescence quantification. Approximately six target peptides were introduced into CHO-PGEA/ED (Figure S3).

Before *in vitro* and *in vivo* delivery, the physicochemical properties of CPC/pCXCL12 and CPC/siR-ICAM1 were investigated using agarose gel electrophoresis, dynamic light scattering, and potential. In addition to CPE, branched PEI (25 kDa), which is the gold standard, was analyzed as a control.[24−26] As shown in Figure 2A, all polycations were fully complexed with nucleic acids when the N/P ratio reached 1.5. All of the polycation/pCXCL12 and polycation/siR-ICAM1 complexes had particle sizes that were suitable for cellular internalization, ranging from 100 to 250 nm (Figure 2B). The nanoparticles became smaller and tighter with increasing N/P ratios because of the more compressed nucleic acids. The best N/P ratio for transfection was 10, as there was no discernible change in the particle size when the N/P ratio was higher than 10 (Figure 2B). The potentials of all complexes were between 20 and 40 mV, which are beneficial for cellular uptake efficiency (Figure 2C). Human serum albumin and other

electronegative substances could reduce the stability of the complexes and cause structural changes. In this study, bovine serum albumin (BSA) was used to treat different polycation/siR-ICAM1 and polycation/pCXCL12 complexes (Figure S4). CPE and CPE showed significantly lower protein adsorption (below 25% at all doses) and better serum tolerance compared to those of PEI/siR-ICAM1 and PEI/pCXCL12, which quickly absorbed over 70% of BSA within 0.5 min. In addition, the sizes of CPE/siR-ICAM1, CPC/siR-ICAM1, CPE/pCXCL12, and CPC/pCXCL12 were fairly constant after 0−5 h of incubation in the serum-containing medium (Figure S5), suggesting the potential for prolonged blood circulation. The better biocompatibility was favored by the many hydroxyl groups of the PGEA-based polycations, in contrast to the numerous irregular amines of the gold standard PEI. Low cytotoxicity and hemolysis ratios were two of the goals of biomaterials. In comparison with PEI/siR-ICAM1 and PEI/pCXCL12 (above 30% at N/P ratio = 10), the cytotoxicity of PGEA-based complexes was considerably lower at various N/P ratios in human umbilical vein ECs (HUVECs) (Figure 2D) due to the abundant hydroxyls.[27] To evaluate blood compatibility, a hemolysis assay was performed. The hemolysis
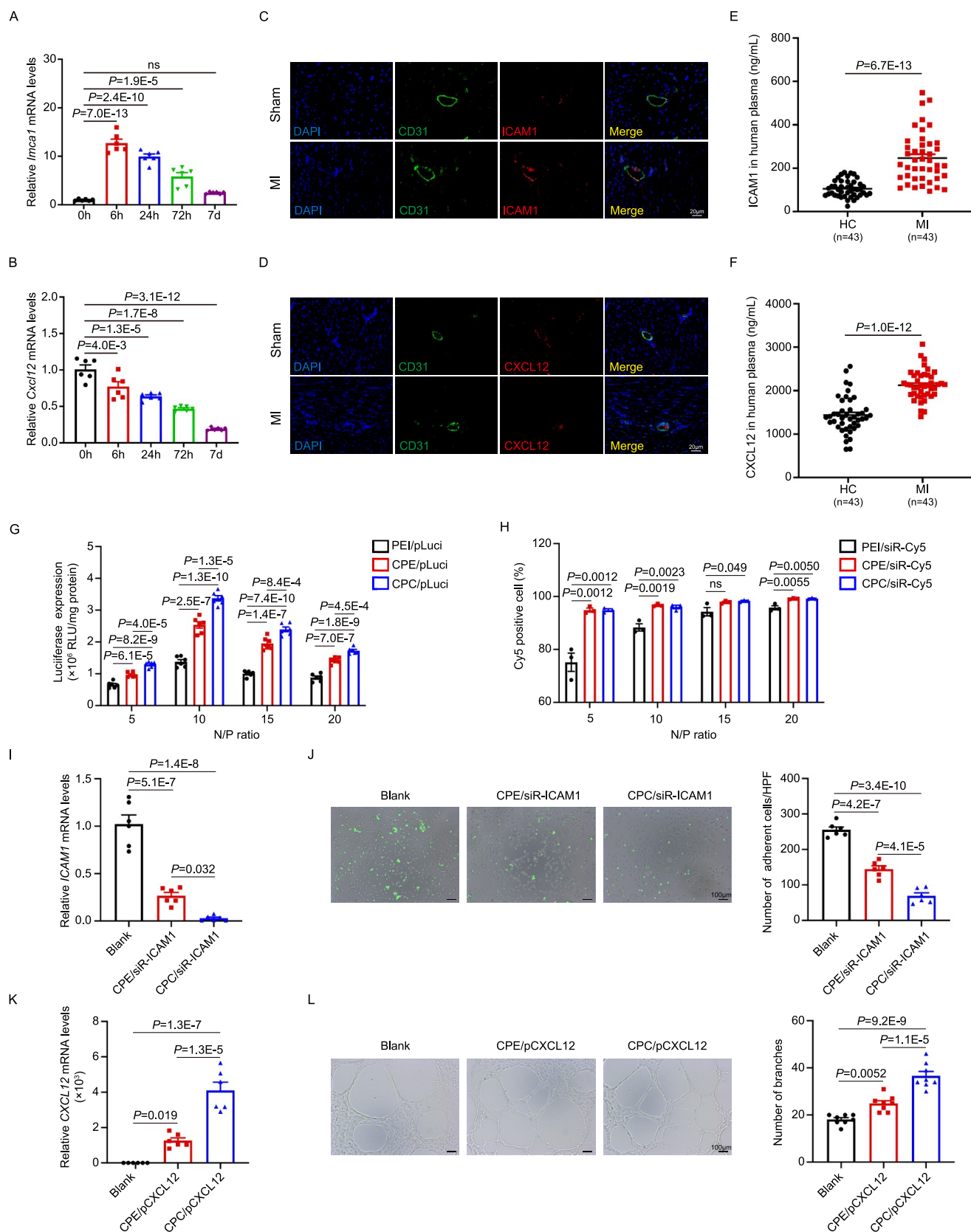
Figure 3. Delivery of pCXCL12 and siR-ICAM1 *in vitro*. (A) Relative mRNA expression of *Icam1* in the heart at different time points after myocardial infarction (MI, *n* = 6 mice per group). **(B)** Relative mRNA expression of *Cxcl12* in the heart at different time points after MI (*n* = 6 mice per group). **(C)** Representative immunostaining of CD31 (green) and ICAM1 (red) in the heart of the Sham and MI groups (*n* = 6 mice per group). Scale bars, 20 *μ*m. **(D)** Representative immunostaining of CD31 (green) and CXCL12 (red) in the heart of the Sham and MI groups (*n* = 6 mice per group). Scale bars, 20 *μ*m. **(E)** Plasma levels of ICAM1 in patients with ischemia (*n* = 43) and age- and sex-matched healthy controls (*n* = 43). **(F)** Plasma levels of CXCL12 in patients with ischemia (*n* = 43) and age- and sex-matched healthy

Figure 3. continued

controls (n = 43). (G) Luciferase expression analysis for cellular uptake efficiency of HUVECs incubated with PEI/pLuci, CPE/pLuci, and CPC/pLuci at different N/P ratios (n = 6 biologically independent samples per group). (H) Flow cytometry analysis of cellular uptake efficiency of HUVECs incubated with PEI/siR-Cy5, CPE/siR-Cy5, and CPC/siR-Cy5 at different N/P ratios (n = 3 biologically independent samples per group). (I) Relative mRNA expression of *ICAM1* in HUVECs treated with CPE/siR-ICAM1 and CPC/siR-ICAM1 (n = 6 biologically independent samples per group). (J) Representative images and quantification of the adhesion assay in HUVECs treated with CPE/siR-ICAM1 and CPC/siR-ICAM1 (n = 6 biologically independent samples per group). HPF, high-power field. (K) Relative mRNA expression of *CXCL12* in HUVECs treated with CPE/pCXCL12 and CPC/pCXCL12 (n = 6 biologically independent samples per group). (L) Representative images and quantification of the tube formation assay in HUVECs treated with CPE/pCXCL12 and CPC/pCXCL12 (n = 6 biologically independent samples per group). Statistical significance was evaluated using an unpaired two-tailed *t*-test (F), unpaired two-tailed Mann−Whitney *U* test (E), and one-way ANOVA, followed by Tukey's multiple comparison test (A, B, H−L). All data are presented as mean $\pm$ SEM.

ratios of CPE and CPC were significantly lower (<5%) than those of PEI (>10%) (Figure 2E). Additionally, the amount of released hemoglobin showed that CPE and CPC had considerably less pronounced hemolytic properties compared to PEI (Figure S6). Red blood cell (RBC) morphology analysis in various groups (Figure 2F) further showed that in contrast to PEI, CPE and CPC did not harm the RBCs structurally. The many hydrophilic hydroxyl groups in CPE and CPC are thought to be responsible for their excellent properties, as they protect the surface from the negative effects of the numerous positive charges.[22,27]

Delivery of pCXCL12 and siR-ICAM1 In Vitro. To elucidate the involvement of ICAM1 and CXCL12 in MI, we examined their dynamic expression in mouse myocardial tissues at different time points after ligation of the left anterior descending artery (LAD). The results showed that *Icam1* was induced early and peaked 6 h after MI, whereas the expression of *Cxcl12* gradually decreased after ischemic injury (Figure 3A,B). Double immunofluorescence staining for ICAM1 or CXCL12 together with CD31 confirmed that ICAM1 and CXCL12 were expressed in cardiac CD31^{+} endothelial cells (Figure 3C,D). Similarly, reverse transcription quantitative real-time polymerase chain reaction (RT-qPCR) showed that *Icam1* and *Cxcl12* were mainly expressed in endothelial cells rather than in cardiomyocytes, cardiac fibroblasts, or macrophages (Figure S7). To investigate the changes in circulating ICAM1 and CXCL12 levels in patients with myocardial ischemia, we measured plasma ICAM1 and CXCL12 levels in patients with acute coronary syndrome (ACS) and previous MI. Age- and sex-matched healthy controls (HCs) were included. The results showed that plasma levels of ICAM1 and CXCL12 were consistently and significantly higher in the ACS group compared to those in the HCs (Figure 3E,F), suggesting that ICAM1 and CXCL12 may be associated with ACS. The above results suggest that targeted endothelial therapy based on ICAM1 and CXCL12 is a promising method for treating myocardial infarction.

Efficient cellular internalization is required for successful gene therapy.[28] The transfection efficiencies of CPE/pLuci and CPC/pLuci nanoparticles were compared with those of PEI/pLuci nanoparticles at different N/P ratios in HUVECs. In the luciferase assay, the CPC/pLuci nanoparticles exhibited a higher gene transfection efficiency than CPE/pLuci and PEI/pLuci nanoparticles (more than 1.3 times). At a N/P ratio of 10, the transfection efficiency was the highest (Figure 3G). The cellular uptake of polycation/siR-Cy5 nanoparticles by HUVECs was also characterized by flow cytometry. The percentage of Cy5-positive cells was higher in the cells treated with CPE/siR-Cy5 and CPC/siR-Cy5 nanoparticles than in

those treated with PEI/siR-Cy5 nanoparticles at different N/P ratios (Figure 3H). Therefore, the N/P ratio of the nanoparticles was set to 10 for subsequent experiments.

After cellular uptake, the expression level of *ICAM1* in HUVECs was examined by RT-qPCR. Compared with that of the blank group, CPE/siR-ICAM1 significantly decreased the expression of *ICAM1*, whereas transfection with CPC/siR-ICAM1 further reduced *ICAM1* levels (Figure 3I). In addition, the beneficial bioactivity of polycation/siR-ICAM1 was investigated using a monocyte-endothelial adhesion assay. The adhesion rate of HUVECs decreased after the addition of CPE/siR-ICAM1 and was further reduced by CPC/siR-ICAM1 (Figure 3J). The relative *CXCL12* expression mediated by CPE/pCXCL12 was also significantly higher than that in the blank group. Importantly, CPC/pCXCL12 was more effective than CPE/pCXCL12 because of the enhanced endocytosis of pCXCL12 (Figure 3K). Angiogenesis is critical for cardiac repair after MI. The direct effects of polycation/pCXCL12 on the ability of HUVECs to form a tube network were examined using an *in vitro* tube formation assay. As shown in Figure 3L, more mature and well-connected capillary tubes were formed in the group transfected with CPC/pCXCL12 than in the blank and CPE/pCXCL12 groups. These results suggest that CPC could effectively introduce siR-ICAM1 and pCXCL12 into HUVECs to exert specific biological functions.

Combinatorial Therapy with siR-ICAM1 and pCXCL12 Using CHO-PGEA on Myocardial Infarction. To further investigate the potential role of *Icam1* and *Cxcl12* intervention in MI, we delivered ICAM1 siRNA (siR-ICAM1, 2.5 nmol/mouse) and CXCL12-overexpressing plasmid (pCXCL12, 25 μg/mouse) by CPE to the heart individually or together 30 min after MI (Figure 4A). Compared with the CPE/siR-negative control (NC), the CPE/siR-ICAM1 group showed a significant decrease in *Icam1* levels in the infarcted heart tissue at different time points (Figure 4B). Additionally, CPE/pCXCL12 increased *Cxcl12* mRNA levels in the infarcted myocardium compared with CPE/empty plasmid (Figure 4C). These results demonstrate that CPE successfully delivered siR-ICAM1 or pCXCL12 into the mouse heart. Subsequently, three therapeutic strategies: CPE/siR-ICAM1, CPE/pCXCL12 alone, and combination therapy (CPE/siR-ICAM1 and CPE/pCXCL12) were examined *in vivo*. Echocardiography showed that all three therapies improved cardiac function as measured by the increase in left ventricular ejection fraction (EF) and fractional shortening (FS) 14 days after MI. The combination therapy of CPE/siR-ICAM1 and CPE/pCXCL12 (CPE/siR-ICAM1+CPE/pCXCL12) demonstrated the most favorable outcome (Figure 4D). The infarct area was distinguished by
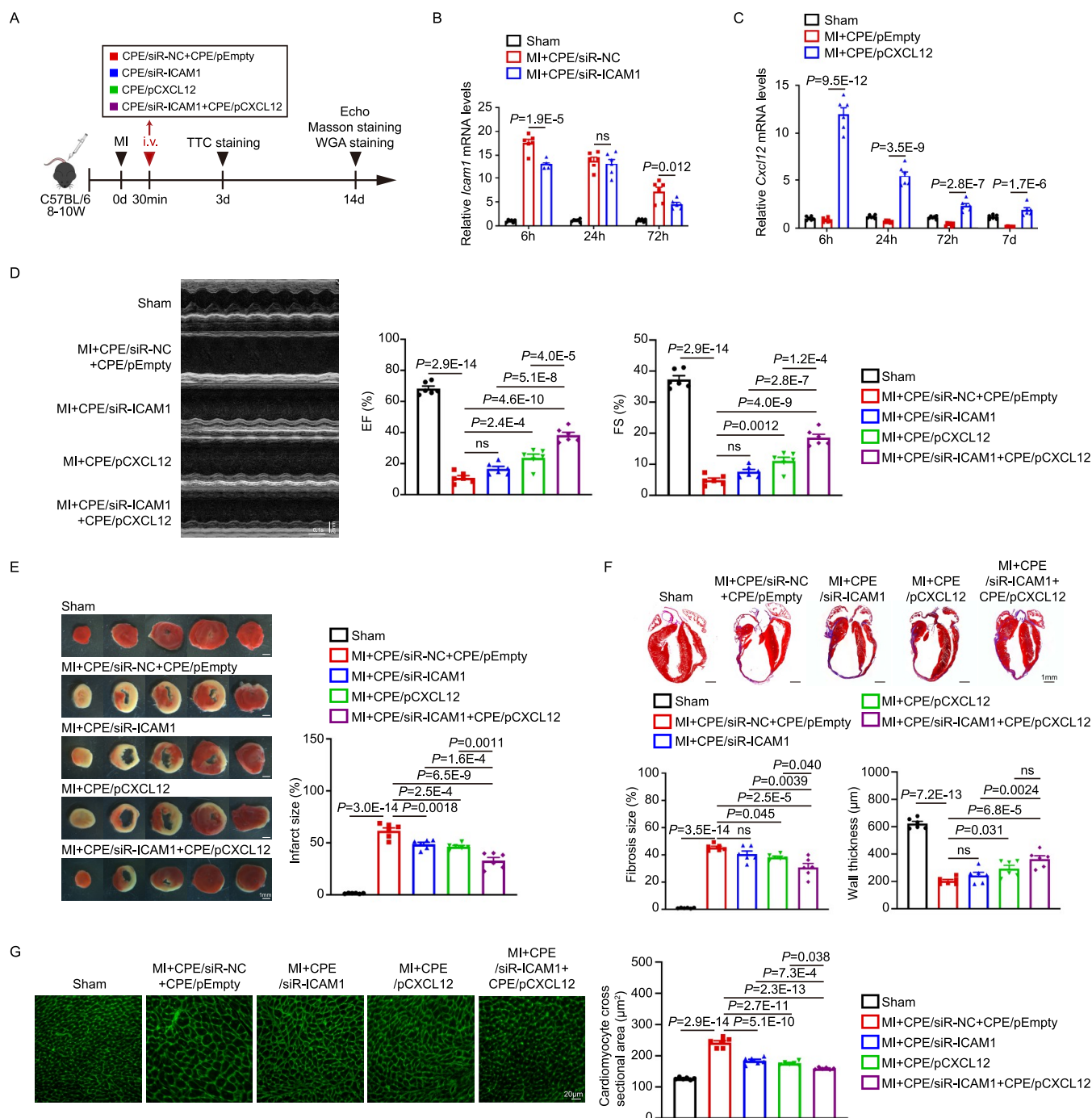
Figure 4. Combinatorial therapy with siR-ICAM1 and pCXCL12 using CHO-PGEA on myocardial infarction. (A) Schematic representation of the *in vivo* experimental design. Male C57BL/6 mice were administered treatment 30 min post-MI and divided into MI+CPE/siR-NC +CPE/pEmpty, MI+CPE/siR-ICAM1, MI+CPE/pCXCL12, and MI+CPE/siR-ICAM1+CPE/pCXCL12 groups. (B) Relative mRNA expression of *Icam1* in the heart at different time points after each complex administration post-MI (*n* = 6 mice per group). (C) Relative mRNA expression of *Cxcl12* in the heart at different time points after each complex administration post-MI (*n* = 6 mice per group). (D) Representative echocardiographic images, EF and FS in the mice administered with each complex 14 days post-MI (*n* = 6 mice per group). (E) Representative images and quantification of 2,3,5-triphenyl tetrazolium chloride staining in hearts administered with each complex 3 days post-MI (*n* = 6 mice per group). Scale bars, 1 mm. (F) Representative images and quantification of Masson's trichrome staining in hearts administered with each complex 14 days post-MI (*n* = 6 mice per group). Scale bars, 1 mm. (G) Representative images and quantification of WGA staining in hearts administered with each complex 14 days post-MI (*n* = 6 mice per group). Scale bars, 1 mm. Statistical significance was evaluated using a one-way ANOVA, followed by Tukey's multiple comparison test (B–G). All data are presented as mean ± SEM.

2,3,5-triphenyl-2H- tetrazolium chloride (TTC) staining of heart sections 3 days after MI. The MI control group exhibited

a larger infarct area than the sham group. The heart sections treated with the three treatments showed a significant
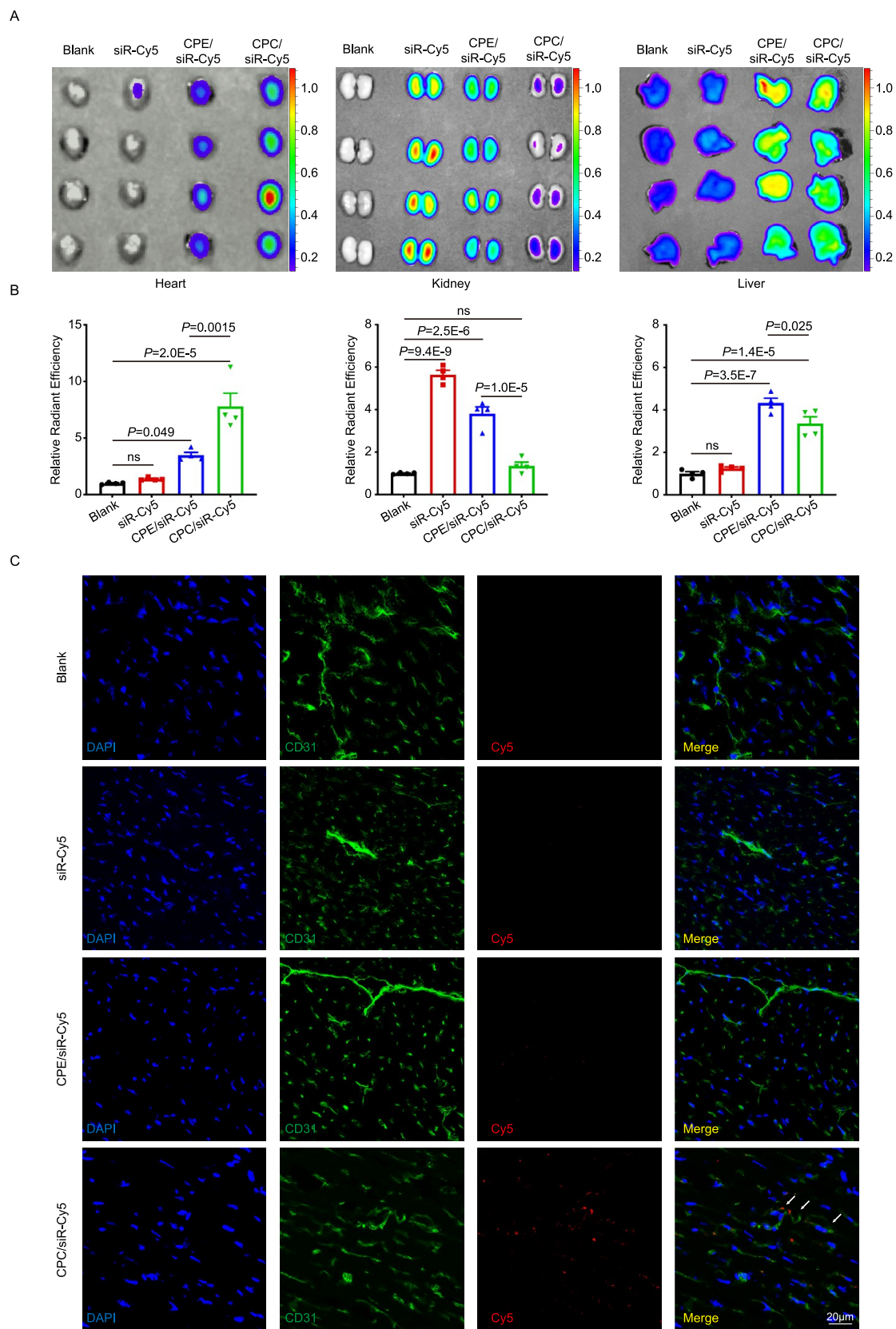
Figure 5. Cardiac targeting capability of CPC. (A) Representative IVIS fluorescence images in mice hearts, livers, and kidneys at 2h after administration with Blank, siR-Cy5, CPE/siR-Cy5, and CPC/siR-Cy5. **(B)** Quantification of fluorescence intensity in the heart, liver, and kidney (*n* = 4 mice per group). **(C)** Representative fluorescence images of CD31 (green) and Cy5 (red) in the heart of the Blank, siR-Cy5, CPE/siR-Cy5, and CPC/siR-Cy5 groups. Scale bars, 20 *μ*m. Statistical significance was evaluated using a one-way analysis of variance, followed by Tukey's multiple comparison test (B). All data are presented as mean ± SEM.
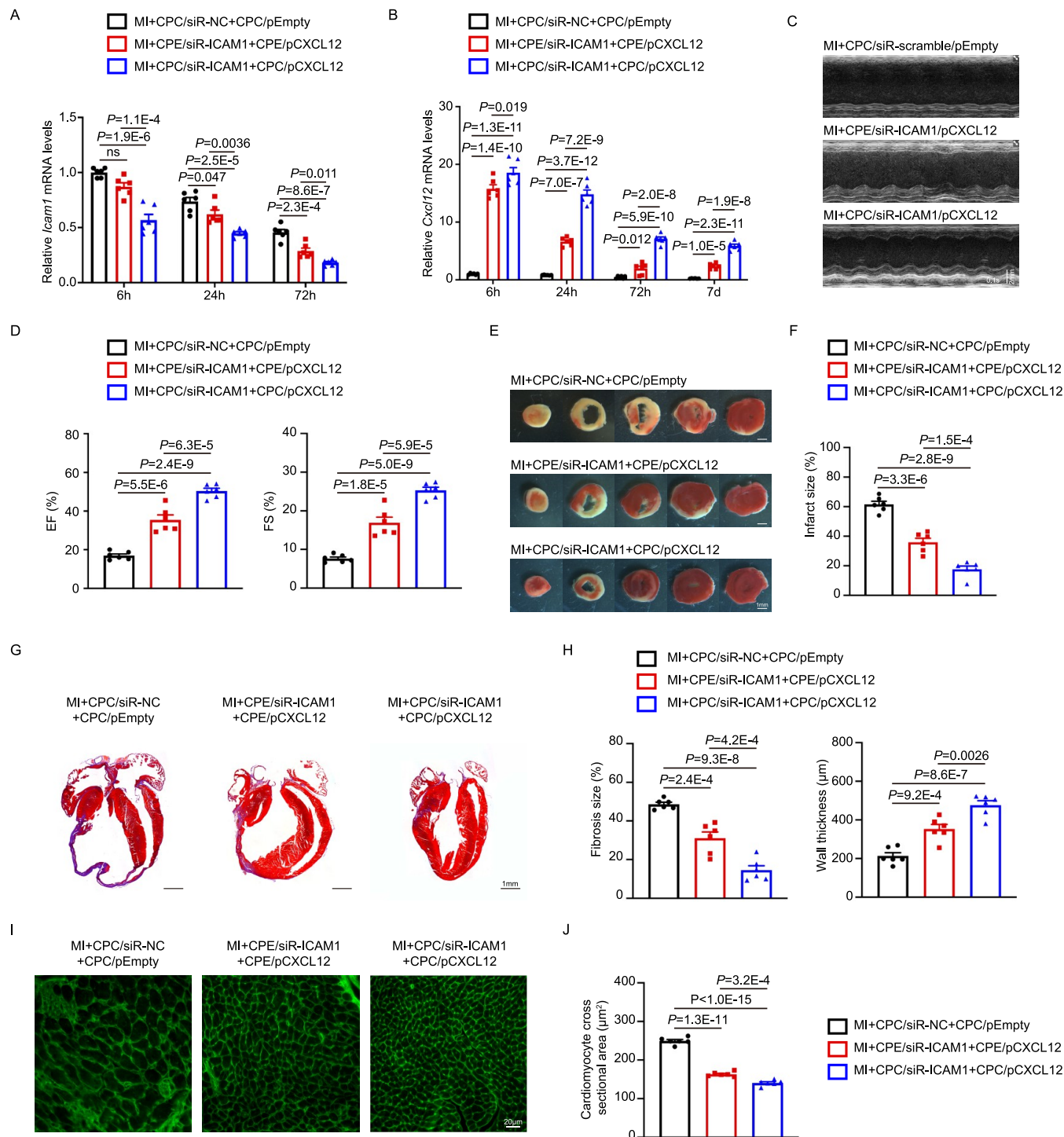
**Figure 6. Targeted therapy of CPC/siR-ICAM1+CPC/pCXCL12 on myocardial infarction. (A) Relative mRNA expression of *Icam1* in hearts at different time points after CPC/siR-NC+CPC/pEmpty, CPE/siR-ICAM1+CPE/pCXCL12, and CPC/siR-ICAM1+CPC/pCXCL12 complexes administration post-MI ($n = 6$ mice per group). (B) Relative mRNA expression of *Cxcl12* in hearts at different time points after each complex administration post-MI ($n = 6$ mice per group). (C, D) Representative echocardiographic images, EF and FS in mice administered each complex 14 d post-MI ($n = 6$ mice per group). (E, F) Representative images and quantification of 2,3,5-triphenyl tetrazolium chloride staining in hearts administered each complex 3 days post-MI ($n = 6$ mice per group). Scale bars, 1 mm. (G, H) Representative images and quantification of Masson's trichrome staining in hearts administered each complex 14 days post-MI ($n = 6$ mice per group). Scale bars, 1 mm. (I, J) Representative images and quantification of WGA staining in hearts administered each complex 14 days post-MI ($n = 6$ mice per group). Scale bars, 1 mm. Statistical significance was evaluated using a one-way ANOVA, followed by Tukey's multiple comparison test (A, B, D, F, H, and J). All data are presented as mean ± SEM.**

H
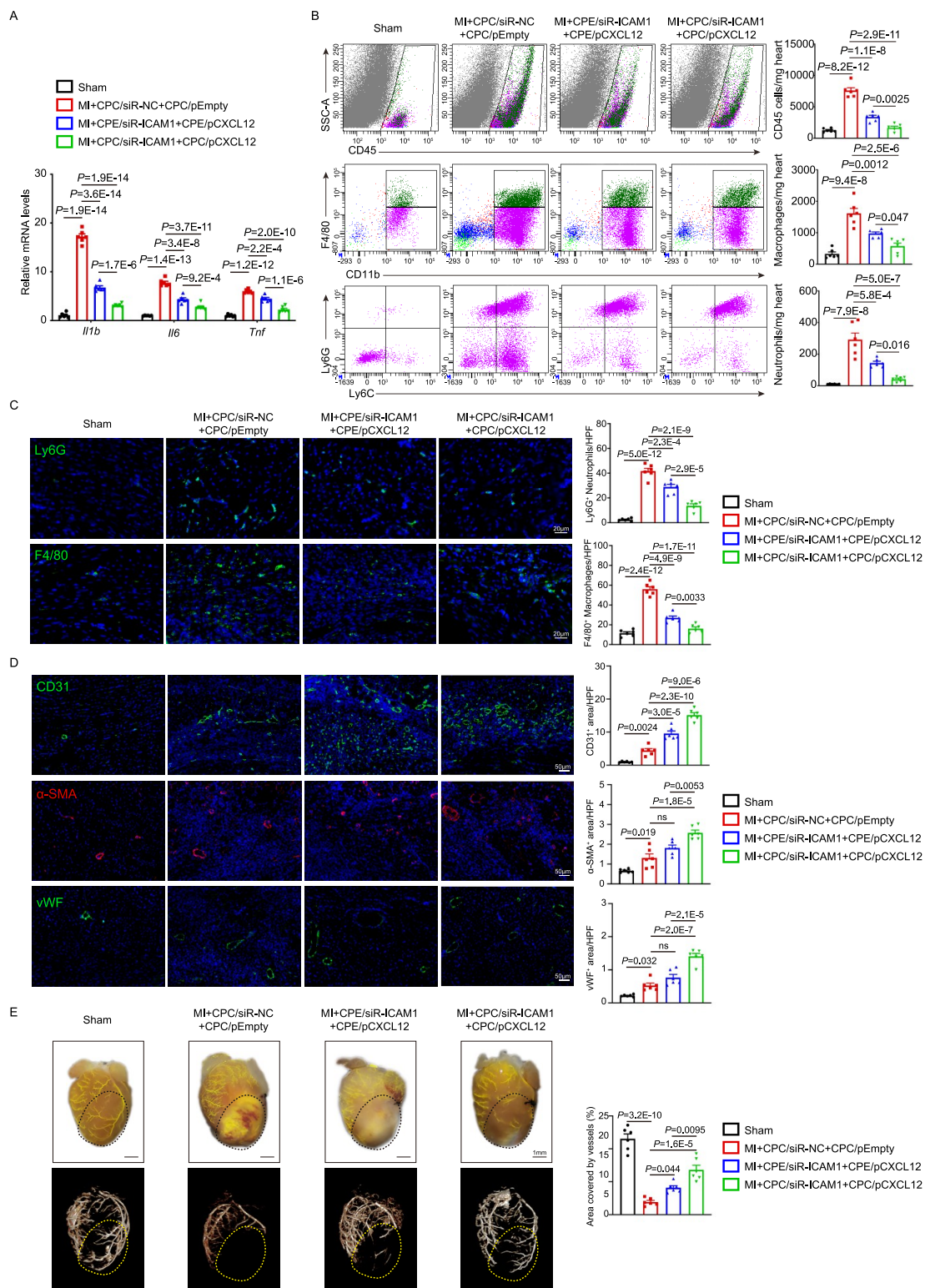
Figure 7. Immunomodulatory and proangiogenic effects of the CPC/siR-ICAM1+CPC/pCXCL12 complex in the infarct region *in vivo*. (A) Relative mRNA expression of *Il1b*, *Il-6*, and *Tnf* in hearts administered with CPC/siR-NC+CPC/pEmpty, CPE/siR-ICAM1+CPE/pCXCL12, and CPC/siR-ICAM1+CPC/pCXCL12 complexes 6 h post-MI (*n* = 6 mice per group). (B) Flow cytometry analysis and quantification of CD45 [+] leukocyte, CD11b^{+}F4/80^{+} macrophage, and Ly6C^{−}Ly6G^{+} neutrophil populations in hearts administered with each complex 6 h post-MI (*n* = 6 mice per group). (C) Representative images and quantification of Ly6G^{+} and F4/80[+] area per high-power field in hearts administered with each complex 6 h post-MI (*n* = 6 mice per group). Scale bars, 20 μm. (D) Representative images and quantification of CD31^{+}, α-SMA^{+}, and vWF^{+} area per high-power field in hearts administered with each complex 14 days post-MI (*n* = 6 mice per group). Scale bars, 50 μm. (E) Representative images and quantification of Microfil vascular casting and microCT in hearts administered with each complex 14 days post-MI (*n* = 6 mice per group). Scale bars, 1 mm. Statistical significance was evaluated using one-way analysis of variance (ANOVA), followed by Tukey's multiple comparison test (A−E). All data are presented as mean ± SEM.

I
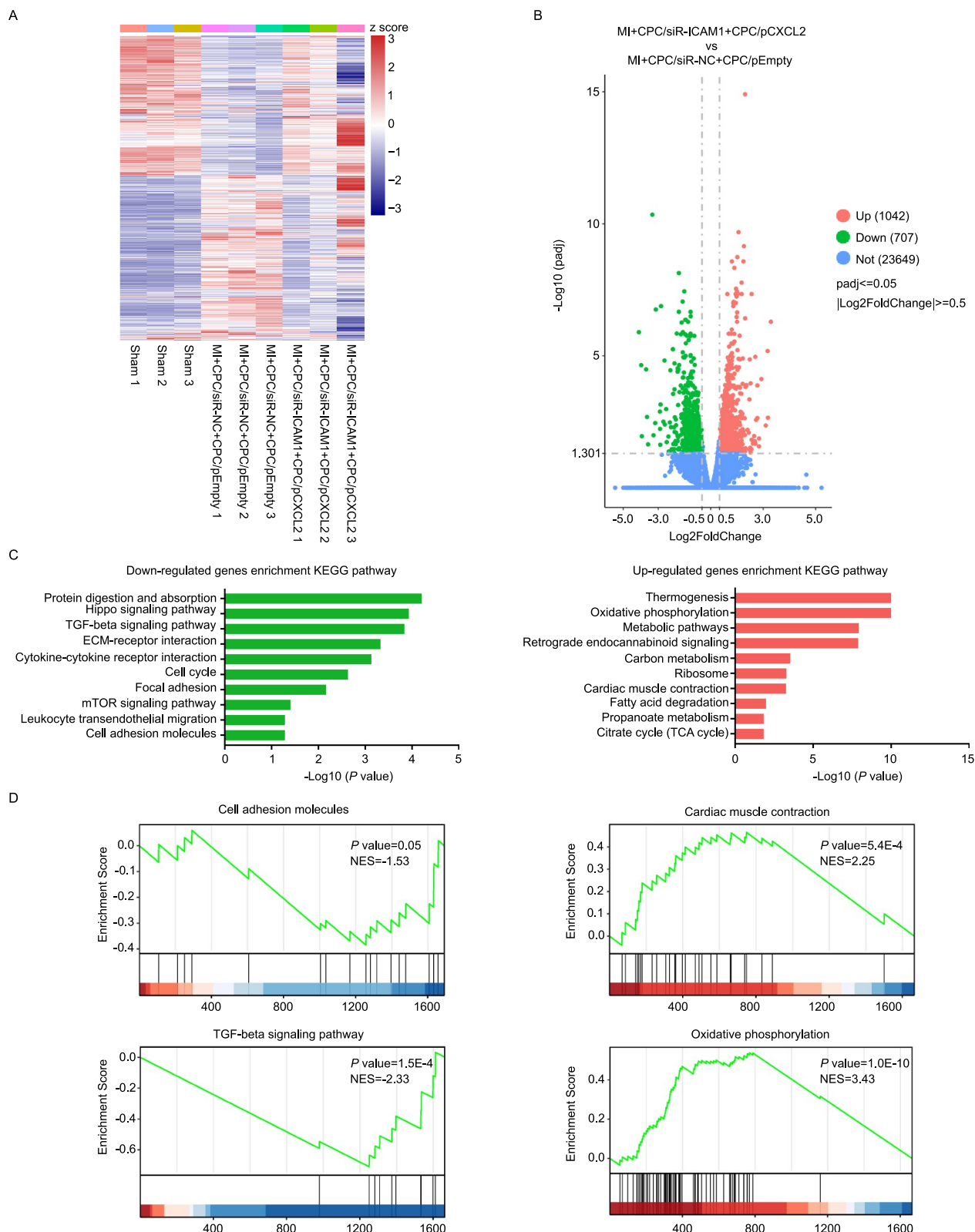
Figure 8. High-resolution transcriptomic profiling of the heart treated with the CPC/siR-ICAM1+CPC/pCXCL12 complex after MI. (A) Hierarchical clustering and heatmap of DEGs in hearts determined by RNaseq of Sham, MI+CPE/siR-NC+CPE/pEmpty, and MI+CPC/siR-ICAM1+CPC/pCXCL12 groups. (B) Volcano plots showing DEGs with |Log2FoldChange| ≥ 0.5 and padj ≤ 0.05 in MI tissue treated with CPE/siR-NC+CPE/pEmpty or CPC/siR-ICAM1+CPC/pCXCL12. The green dots indicate downregulated DEGs. The red dots indicate upregulated DEGs. (C) GSEA analysis of significantly down- and upregulated genes in MI+CPC/siR-ICAM1+CPC/pCXCL12 compared with MI+CPE/siR-NC+CPE/pEmpty is shown. (D) GSEA analysis showed that cell adhesion molecules and TGF-beta signaling pathway were downregulated and cardiac muscle conreaction and oxidative phosphorylation were upregulated in MI+CPC/siR-ICAM1+CPC/pCXCL12 compared with MI+CPE/siR-NC+CPE/pEmpty at day 3 after MI. NES, normalized enrichment score.

reduction in infarct size compared to the MI+CPE/siR-NC +CPE/pEmpty group. The combined administration exhibited an enhanced therapeutic effect compared with individual administrations (Figure 4E). Cardiac tissue morphology and fibrosis size were assessed 14 days after MI using Masson's trichrome staining. Among the three different groups, the combination therapy group showed the best therapeutic effect in terms of fibrosis size and thickness compared to those of the other single regimens (Figure 4F). Moreover, the combination regimen showed a significantly better protective effect against myocardial hypertrophy than that of CPE/siR-ICAM1 or CPE/pCXCL12 alone after MI (Figure 4G). Overall, the combination therapy had a stronger targeted therapeutic effect than CPE/siR-ICAM1 or CPE/pCXCL12 in MI mice.

Cardiac Targeting Capability of CPC. Although the combination of CPE/siR-ICAM1 and CPE/pCXCL12 plays a protective role in reducing myocardial necrosis, improving cardiac function, and inhibiting cardiac remodeling to a certain extent, its clinical utility is limited because of subpar targeting when administered systemically. Next, we evaluated the delivery efficiency of CPC nanoparticles *in vivo*. Free siR-Cy5, CPE/siR-Cy5, and CPC/siR-Cy5 nanoparticles were administered to C57BL/6J mice by intravenous injection. Two hours after injection, various organs (heart, kidneys, and liver) were harvested, and the siR-Cy5 fluorescence intensity in these organs was imaged and analyzed using the IVIS imaging system. Representative IVIS images show that the fluorescence intensity in the heart tissue of the CPC/siR-Cy5 group was significantly higher than that of the free siR-Cy5 and CPE/siR-Cy5 groups. Conversely, the fluorescence intensity in organs other than the heart (kidneys and liver) was significantly higher in the CPE/siR-Cy5 group than in the CPC/siR-Cy5 group. The fluorescence intensity emitted by siR-Cy5 was detected by drawing a region of interest (ROI) and quantified by the relative radiation efficiency. Cardiac fluorescence intensity increased by more than 2-fold in the CPC/siR-Cy5 group compared with that in the CPE/siR-Cy5 group (Figure 5A). In addition, fluorescence images of heart sections from different groups were obtained using confocal laser scanning microscopy (CLSM) to observe the cellular uptake of siR-Cy5. ECs in the vessels were stained green by immunofluorescent staining for CD31. The accumulation of Cy5 from the CPC/siR-Cy5 group was significantly enriched in ECs compared with that in the free siR-Cy5 and CPE/siR-Cy5 groups (Figure 5B). These results demonstrate that CPC/siR-Cy5 specifically transports siR-Cy5 into cardiac ECs.

Targeted Therapy of CPC/siR-ICAM1+CPC/pCXCL12 on Myocardial Infarction. To investigate the therapeutic effects of intravenously administered CPC/siR-ICAM1+CPC/ pCXCL12 in mice post-MI, we examined the expression levels of *Icam1* and *Cxcl12* in each group. The CPE/siR-ICAM1+CPE/pCXCL12 and CPC/siR-ICAM1+CPC/ pCXCL12 groups showed significantly reduced expression of *Icam1* and enhanced expression of *Cxcl12* in cardiac tissues at different time points post-MI. These effects were more pronounced in the CPC/siR-ICAM1+CPC/pCXCL12 group (Figure 6A,B). C57BL/6J mice were randomly assigned to three groups: CPC/siR-NC/pEmpty (control), CPE/siR-ICAM1+CPE/pCXCL12, or CPC/siR-ICAM1+CPC/ pCXCL12. Cardiac function was determined by echocardiography 14 days after the MI. The CPC/siR-ICAM1+CPC/ pCXCL12 complexes improved cardiac function, characterized by increased EF and FS, compared to the control and CPE/

siR-ICAM1+CPE/pCXCL12 groups (Figure 6C,D). Infarct size measured by TTC staining revealed that the group injected with CPC/siR-ICAM1+CPC/pCXCL12 had the smallest infarct size (Figure 6E,F). Masson's trichrome staining showed that injection of CPC/siR-ICAM1+CPC/pCXCL12 complexes decreased the size of fibrosis and increased the thickness of the infarcted left ventricular wall compared to the control and CPE/siR-ICAM1+CPE/pCXCL12 groups (Figure 6G,H). Wheat germ agglutinin (WGA) staining was performed to evaluate the cardiomyocyte hypertrophy. The CPC/siR-ICAM1+CPC/pCXCL12 complexes significantly inhibited myocardial hypertrophy compared to the other groups (Figure 6I,J). Overall, the CPC/siR-ICAM1+CPC/pCXCL12 complex exerted a stronger therapeutic effect than did the CPE/siR-ICAM1+CPE/pCXCL12 complex in MI mice.

Anti-Inflammatory and Proangiogenic Effects of the CPC/siR-ICAM1+CPC/pCXCL12 Complex after MI. To investigate the therapeutic mechanisms by which CPC/siR-ICAM1+CPC/pCXCL12 complexes promote cardiac function, the expression levels of inflammatory factors were examined after administration to each group. CPC/siR-ICAM1+CPC/pCXCL12 significantly reduced the mRNA expression levels of *Il1b*, *Il6*, and *Tnf* (Figure 7A). Flow cytometry was used to examine the infiltration of inflammatory cells in infarcted hearts at 3 days post-MI. Compared with sham treatment, MI dramatically increased the number of F4/ 80$^+$ macrophages and Ly6G$^+$ neutrophils (Figure 7B). The CPC/siR-ICAM1+CPC/CXCL12 group had significantly fewer F4/80$^+$ macrophages and Ly6G$^+$ neutrophils than the control and CPE/siR-ICAM1+CPE/pCXCL12 groups (Figure 7B). These results were further verified by immunofluorescence staining of F4/80 or Ly6G in heart sections 3 days post-MI (Figure 7C). We examined the proreparative effect of CPC/siR-ICAM1+CPC/pCXCL12 complexes in the ischemic myocardium. Immunofluorescence staining of the vascular markers CD31, α-SMA, and vWF showed that the arterial density was significantly higher in the CPC/siR-ICAM1+CPC/pCXCL12 group than in the CPE/siR-ICAM1+CPE/pCXCL12 group on day 14 post-MI (Figure 7D). Similarly, 3D visualization of the coronary arterial vascular network via microcomputed tomography (micro-CT) imaging on day 14 post-MI demonstrated marked angiogenesis in the CPC/siR-ICAM1+CPC/CXCL12 group compared to that in the control and CPE/siR-ICAM1+CPE/ pCXCL12 groups (Figure 7E).

High-Resolution Transcriptomic Profiling of the Heart Treated with the CPC/siR-ICAM1+CPC/pCXCL12 Complex after MI. In parallel, the transcriptome changes in the hearts of the sham, CPE/siR-NC+CPE/pEmpty and CPC/ siR-ICAM1+CPC/pCXCL12 groups on day 3 after MI were analyzed simultaneously by RNA sequencing (RNaseq). Hierarchical clustering analysis of the RNaseq data revealed significant differences in gene signatures among the three groups (Figure 8A). As shown by the volcano plot, 1042 genes were upregulated and 707 genes were downregulated in the CPC/siR-ICAM1+CPC/pCXCL12 treatment group compared with the control group (|Log2FoldChange| $\geq$ 0.5, padj $\leq$ 0.05; Figure 8B). Gene set enrichment analysis (GSEA) showed that treatment with CPC/siR-ICAM1+CPC/ pCXCL12 resulted in a reduction in the inflammatory infiltration and fibrosis process, as indicated by downregulated cell adhesion molecules (CAMs) and TGF-beta signaling pathway. The most upregulated pathways in CPC/siR-

ICAM1+CPC/pCXCL12-treated mice included cardiac muscle contraction and energy metabolism (Figure 8C,D).

For the CPC/siR-ICAM1+CPC/pCXCL12 complex to be used *in vivo*, its toxicity in other organs must be investigated.[27] Morphological changes in the liver, kidney, and lungs were examined by hematoxylin and eosin (H&E) staining after *in vivo* therapy in each group. Blinded histopathology scoring analysis revealed no significant pathological abnormalities (Figure S8A). The mice's levels of albumin (ALB), blood urea nitrogen (BUN), creatinine (CRE), aspartate aminotransferase (AST), alanine aminotransferase (ALT), total bilirubin (TBIL), and albumin (ALB) remained normal 24 h after injection of the CPC/siR-ICAM1+CPC/pCXCL12 complex (Figure S8B). This finding indicated that no acute damage occurred in the liver, kidneys, or lungs. These results demonstrate the safety of the CPC/siR-ICAM1+CPC/pCXCL12 complex and its promising *in vivo* applications.

DISCUSSION

In the present study, we developed an efficient therapeutic strategy for cardiac repair using a cardiac EC-targeting nanosystem to deliver a combination of siR-ICAM1 and pCXCL12 after MI. We showed that the combined administration of CPE/siR-ICAM1 and CPE/pCXCL12 immediately after MI resulted in additive cardioprotection and preserved ventricular function in the long term. Subsequently, cardiac endothelial peptide CRPPR was conjugated to the surface of CPE to enhance nucleic acid drug accumulation in the cardiac endothelium. Moreover, CPC/siR-ICAM1+CPC/pCXCL12 effectively protected against cardiac injury by inhibiting inflammatory cell infiltration and promoting angiogenesis post-MI.

Multiple pathogenic mechanisms contribute to MI damage, and postischemic microvascular dysfunction is exacerbated by leukocyte adhesion and inflammation in ECs. Inhibition of leukocyte adhesion to ECs by antagonizing ICAM1 is an effective therapeutic strategy for attenuating myocardial ischemic injury.[29] A study of knockdown of endothelial CAMs by siRNA targeting demonstrated effective inhibition of leukocyte recruitment to the ischemic myocardium and improvement in contractile function as indicated by higher LVEF (siCAM5, 33 ± 4% vs siCtrl, 23 ± 4%) after MI.[12] CXCL12 may limit the infarct size and improve post-MI cardiac function through pleiotropic mechanisms.[30−32] Overexpression of CXCL12 has been shown to induce dramatic expansion of arterial ECs to establish a collateral arterial network, with an improvement in LVEF by approximately 15%.[18] We simultaneously intervened with both molecules, fully demonstrating the stronger effect of the combination in the MI treatment. LVEF was improved by approximately 27% by the codelivery of siR-ICAM1 and pCXCL12, which was superior to any of the individual deliveries. To overcome nonspecific delivery, CRPPR was conjugated to the surfaces of nanoparticles. Notably, the targeted delivery group exhibited the strongest therapeutic effects, with an improvement in the LVEF of approximately 39%, which was close to normal.

Currently, more studies are attempting to use small-molecule agents and other biologics, such as therapeutic transgenes, miRNAs, and siRNAs, for MI therapeutics.[33−35] The clinical utility of these therapeutic agents is limited because they cannot be administered in an organ-specific manner, resulting in their uptake by organs with high blood flow (lungs, liver, and kidneys), whereas their concentrations in the heart are insufficient.[36,37] Nonspecific use in all cell types leads to more severe adverse side effects.[38] The primary role of CXCL12 is to promote angiogenesis, and nontargeted administration of CXCL12 may cause systemic multiorgan angiogenesis characterized by easy bleeding.[39,40] Patients with MI who routinely take aspirin and clopidogrel after surgery are at risk of gastrointestinal bleeding or cerebral hemorrhage.[41,42] Therefore, the nonspecific administration of angiogenic agents may exacerbate the risk of bleeding in these patients. For example, systemic angiogenesis increases the risk of post-diabetic retinal hemorrhage.[43] In another study, VEGFA gene transfer resulted in tissue edema and transient electrolyte changes such as hyponatremia, hyperkalemia, and hypocalcemia.[44] Therefore, it is necessary to target CXCL12 in the cardiac ECs of patients with ischemic heart disease to improve their efficacy and reduce side effects during MI treatment.

Cardiac-targeted delivery has historically been divided into passive and active cardiac targeting.[45] The primary mechanism underlying passive targeting is the enhanced permeability and retention (EPR) effect.[46] The EPR effect, in which tissue vessels become increasingly permeable after injury, can occur at all stages of the pathological process of MI. This allows passive targeted delivery of therapeutic drugs to injured tissues. David et al. studied the biodistribution of nanoparticles of different sizes 30 min after administration. They found that nanoparticles with a diameter of 20−200 nm were optimal for passive targeting of the injured left ventricle.[47] Cardiac active targeting is based on biological targeting, such as antigen−antibody and receptor−ligand targeting, for the final refinement of the tissue and cell specificities of the nanocarriers. The entire infarct region, the cells that make up the arteries, and the cells involved in the postinfarct inflammatory process are all targeted to the heart. For example, Zhao et al. bound primary cardiomyocyte-specific peptides (PCM) to the surface of nanoparticles and demonstrated efficient delivery targeting the heart and effective cardioprotection.[48] In another study, a therapeutic nanosystem (PP/PS @MIONs) was developed for the early treatment of MI. This nanosystem accelerates the elimination of early inflammatory responses by targeting macrophages in the infarct region through PS and an external magnetic field.[49] However, cardiac endothelium has not been considered an active target for delivering therapeutics to treat MI.

CONCLUSION

In summary, combination therapy with siR-ICAM1 and pCXCL12 effectively alleviated the inflammatory response, promoted angiogenesis, and improved cardiac function without any side effects. Our study provides a promising therapeutic and drug delivery approach for cardiovascular diseases.

MATERIALS AND METHODS

Materials. Cholesterol (CHO, 95%), glycidyl methacrylate (GMA, 98%), branched polyethylenimine (PEI, $M_w \sim 25000$ Da), 2-bromoisobutyryl bromide (BIBB, 98%), N,N,N',N'',N''-pentamethyl-diethylenetriamine (PMDETA, 99%), ethanolamine (EA, 98%), and copper(I) bromide (CuBr, 99%) were obtained from Energy Chemical Co. (Shanghai, China). GMA was prepared by the removal of the inhibitors. Cardiac endothelial-targeting peptide CRPPR and rhodamine B-modified CRPPR were purchased from SciLight Biotechnology Co. (Beijing, China).

Synthesis of CHO-PGMA and CPE. The ring-opening reaction of EA and atom transfer radical polymerization (ATRP) of GMA were combined to produce the proposed CHO-PGMA and CHO-PGEA

Table 1. RT-qPCR Primers Used in This Study

gene name	forward primer 5′-3′	reverse primer 5′-3′
Gapdh	AATGCATCCTGCACCACC	ATGCCAGTGAGCTTCCCG
Icam1	CCATCCATCCCAGAGAAGCC	CACTGAGTCTCCAAGCCCAG
Cxcl12	TGCATCAGTGACGGTAAACCA	TTCTTCAGCCGTGCAACAATC
Il1b	GCAACTGTTCCTGAACTCAACT	ATCTTTTGGGGTCCGTCAACT
Il6	TAGTCCTTCCTACCCCAATTTCC	TTGGTCCTTAGCCACTCCTTC
Tnf	CCTGTAGCCCACGTCGTAG	GGGAGTAGACAAGGTACAACCC
ICAM1	ATGCCCAGACATCTGTGTCC	GGGGTCTCTATGCCCAACAA
CXCL12	ATTCTCAACACTCCAAACTGTGC	ACTTTAGCTTCGGGGTCAATGC

(CPE). CHO-terminated poly(glycidyl methacrylate) (CHO-PGMA, $M_n = 9.70 \times 10^3$ g mol^{-1} with PDI of 1.25) and the corresponding CPE were prepared as reported (PGMA-based gene carriers with lipid molecules, 2016 Biomaterials Science).

Synthesis of CHO-PGEA/ED, CPC, and CPC-RhB. For the preparation of CHO-PGEA/ED, CHO-PGMA (100 mg, 0.0104 mmol) was diluted in 5 mL of dimethyl sulfoxide. The system was degassed with nitrogen for 5 min, and then 0.2 mL of ED and 1.8 mL of EA were added. The reaction mixture was stirred at 80 °C for 2 h before lyophilization. The resulting crude CHO-PGEA/ED was purified by using a dialysis membrane (MWCO 1000).

To produce CHO-PGEA/ED-CRPPR (CPC) and CHO-PGEA/ED-CRPPR-RhB (CPC-RhB), 20 mg of CRPPR or 40 mg of rhodamine B-modified CRPPR were dissolved in 2 mL of deionized water containing 6.0 mg of EDC·HCl and 3.6 mg of NHS, respectively. Each reaction mixture was stirred at room temperature. After 1 h, 24 mg of CHO-PGEA/ED was added, and the system was stirred for another day. Subsequently, the CPC and CPC-RhB products were purified using a dialysis membrane (MWCO 10000) before lyophilization.

Simulated System. All MD simulations were performed with GROMACS 2022.1,[50] and the amber99sb-ildn[51] force field was used. The DNA molecule was constructed with reference to a previous study[52] and the sequence d (5′-CGCGAATTCGCGATATCCCGG-3′) was selected to build a B-form DNA duplex with 42 bases and −40 net charge. The CPC1, CPC6, and CPC12 with different CRPPR contents were built using GaussView 5 and the charge of repeat units was calculated using Gaussian 16 with B3LYP/6-31G** (Gaussian 16, rev. A.01). Sobtop 1.0 (http://sobereva.com/soft/Sobtop) and Multiwfn[53] were used to obtain .gro and .top profile for simulation.

The simulation box of the system was constructed with the dimensions $20 \times 20 \times 12$ nm^3, and the DNA was placed at the center of the box. Initially, seven polymers at an N/P ratio of 10 were randomly placed into the box around the DNA. The OPC3[54] water model was used to fill the box and appropriate amounts of chloride ion were used to neutralize the system charge. The energy minimization was initially performed for 100 ps followed by 30 ns of simulation at a constant pressure of 1 bar and a temperature of 298.15 K. Periodic boundary conditions were employed, and the particle-mesh Ewald method[55] was utilized to account for long-range electrostatic interactions. The time step used was 1 fs. The structure of the polymers interacted with DNA, and DNA was extracted for analysis. Pymol was used to present the simulation snapshots.

Physicochemical Characterization. ^{1}H NMR spectra were acquired on a Bruker ARX 400 MHz spectrometer using CDCl$_3$ (for CHO-Br and CHO-PGMA) and D$_2$O (for CPE, CHO-PGEA/ED, and CPC) as solvents, and tetramethylsilane (Me$_4$Si) served as the internal standard. The GPC analysis of CHO-PGMA were conducted using a Waters GPC system with DMSO as the eluent. The fluorescence intensities of the rhodamine B-modified CRPPR and CRPPR-RhB were determined by using a fluorescence spectrophotometer. The dynamic light scattering (DLS) measurements of the polycation/pDNA and polycation/siRNA complexes were carried out by using a Zetasizer Nano ZS.

Gel electrophoresis was conducted using a subcell system from Bio-Rad Laboratories. Additionally, a UV transilluminator and BioDco-It

imaging system from UVP Inc. were utilized to visualize the pDNA and siRNA bands.

Protein Absorption and Particle Size Stability Assay. In the protein absorption assay, 100 μL of CPE solution (2.12 mg/mL), 100 μL of CPC solution (2.12 mg/mL), and 100 μL of PEI solution (0.43 mg/mL) were each combined with 100 μL of nucleic acid solution (0.33 mg/mL). The mixtures were incubated for 30 min to form complexes. Subsequently, 40 μL of bovine serum albumin (BSA) solution (2 mg/mL) was added to the complex solution and shaken at 37 °C for durations ranging from 0.5 to 60 min. After high-speed centrifugation, the supernatant was collected to separate the protein complexes from the polycations. The concentration of BSA in the supernatant was determined using the BCA protein assay.

To evaluate particle size stability, complexes were prepared with an N/P ratio of 10 by mixing the polycation-containing solution with miRNA solution (5 μg) for 30 min before use. The complexes were then added to 800 μL of 10% DMEM, and the particle sizes were assessed over an incubation period of 0−5 h.

Hemolysis Assay. Hemolysis assays were performed using the blood of C57BL/6 mice (ViewSolid Biotech, Stock No: VSM10001, Beijing, China). The RBCs were prepared as described previously. CPE, CPC, and PEI were added to 2% RBCs suspension at 0.1 mg mL^{-1} and 1 mg mL^{-1}, respectively. Furthermore, RBCs treated with deionized water and PBS were employed as positive and negative controls, respectively. Calculation of the hemolysis ratio and collection of corresponding confocal images have been described in detail previously.[27]

Animal Studies. Male C57BL/6 mice, aged 10−12 weeks, were obtained from View Solid Biotechnology (Beijing, China). Throughout the study, all mice were housed in a pathogen-free environment with ad libitum access to food and water. The room was maintained at a constant temperature (20−25 °C) and humidity level (30−70%), and a standard light cycle of 12 h of light and 12 h of darkness was implemented. All animal procedures adhered to the Guidelines on the Use and Care of Laboratory Animals and received approval from the Animal Subjects Committee of Beijing Anzhen Hospital, Capital Medical University.

Mouse MI Model and In Vivo Treatment. MI was induced through permanent ligation of the LAD coronary artery, as previously described.[56] In brief, male C57BL/6 mice aged 10−12 weeks were anesthetized with 2−3% isoflurane in oxygen. Access to the heart was obtained through the third intercostal space on the left side, and the LAD coronary artery was ligated 2−3 mm from its origin using a 6−0 silk suture. Ischemia was confirmed through electrocardiography (ST-segment elevation) and observation of the myocardial color changes. Sham-operated mice underwent the same procedure without LAD ligation. Thirty minutes postmyocardial ischemia, complexes including CPE/siR-NC+CPE/pEmpty, CPE/siR-ICAM1, CPE/pCXCL12, CPE/siR-ICAM1+CPE/pCXCL12, or CPC/siR-ICAM1+CPC/pCXCL12 were administered via intracanthal vein injection. Each injection comprised 2.5 nmol of siRNA and 25 μg of pDNA, with a total volume of 100 μL.

In Vivo Fluorescent Imaging. Four groups of 16 male C57BL/6J mice were randomly divided: three experimental groups and one blank control group. The control group received intravenous injections of saline, while the other groups were administered siR-Cy5, CPE/siR-Cy5, or the CPC/siR-Cy5 complex. The complex had

an N/P ratio of 10, and a 100 μL injection containing 5 nmol of siR-Cy5 was administered. Fluorescence signals of the polymer/siR-Cy5 complexes in the heart, kidney, and liver were recorded using the Xenogen IVIS imaging system (U.S.A.) and Living Image 2.11 software, 2 h postadministration. To assess the invasion of polycation/siR-Cy5 complexes into mouse hearts, mouse heart sections were examined using CLSM.[22]

Reverse Transcription Quantitative Real-Time PCR (RT-qPCR). Total RNA from cardiac tissue and cultured cells was isolated using TRIzol reagent (Invitrogen, Carlsbad, CA, U.S.A.), followed by chloroform extraction. Subsequently, 2 μg of total RNA underwent cDNA synthesis using a reverse transcription kit (Promega, Madison, WI, U.S.A.). RT-qPCR was then conducted using the SYBR Green PCR Master Mix (TaKaRa, Shiga, Japan) on an iCycler iQ system (Bio-Rad). The relative expression level of each mRNA was determined utilizing the $2^{-\Delta\Delta CT}$ cycle threshold method and normalized to *Gapdh* mRNA.[57]

RT-qPCR primers used in this study can be seen in Table 1.

Immunofluorescence. Mouse hearts were perfused, fixed in 10% formalin, embedded in paraffin, and sectioned continuously at a thickness of 4 mm. Dewaxed heart sections underwent antigen retrieval in citrate buffer (pH 6.0) or EDTA buffer (pH 9.0) for 15 min. Cells were fixed with prechilled methanol for 10 min, washed twice with PBS at 5 min intervals, and permeabilized with 0.1% Triton X-100 in PBS for 10 min at room temperature.

Sections and cells were blocked with 5% BSA/PBS for 1 h at room temperature and then incubated overnight at 4 °C with primary antibodies in 3% BSA/PBS, including anti-ICAM1 (Santa Cruz sc-107; 1:100), anti-SDF-1 (Santa Cruz sc-74271; 1:100), anti-CD31 (Abcam ab222783; 1:100), anti-α-SMA (Abcam ab208638; 1:100), anti-VWF (Abcam ab11713; 1:100), anti-LY6G (Abcam ab25377; 1:100), and anti-F4/80 (Abcam, ab6640; 1:100). Stained sections and cells were then washed with PBS and incubated with secondary antibodies conjugated to Alexa Fluor 488 or Alexa Fluor 555 (Invitrogen; 1:500) for 1 h at room temperature in 1% BSA/PBS. Nuclei were stained with DAPI (Abcam, ab104139). Immunofluorescence images were acquired using a Leica ST5 laser scanning confocal microscope.[58]

Enzyme-Linked Immunosorbent Assay (ELISA). Plasma ICAM1 and CXCL12 levels were assessed using a human ICAM1 Quantikine ELISA kit (DCD540, R&D Systems) and a human CXCL12 Quantikine ELISA kit (DSA00, R&D Systems), respectively, following the manufacturer's instructions. All measurements were conducted in duplicate.[59]

Echocardiography. Transthoracic echocardiographic analysis was performed on conscious mice 2 weeks postsham or myocardial infarction (MI) using a VisualSonics Vevo 2100 Ultrasound system (Visual Sonics, Canada) with a 30 MHz linear array transducer. Mice were anesthetized with 2–3% isoflurane in oxygen and positioned on a heating plate in the supine position. Two-dimensional M-mode guided measurements were taken for the anterior and posterior wall thicknesses at the end diastole and end systole. The left ventricular (LV) internal diameter (LVID) was determined by measuring the largest anteroposterior diameter during diastole (LVIDd) or systole (LVIDs). Left ventricular ejection fraction (LVEF) data were calculated as described previously.[60]

Triphenyl Tetrazolium Chloride (TTC) Staining. At 72 h post MI, mice were euthanized, and their hearts were rapidly frozen at −80 °C for 30 min. The entire heart was excised, frozen again at −80 °C for 30 min, and then sliced into five 1.0 mm thick sections perpendicular to the long axis. These sections were incubated with freshly prepared 1% TTC (Sigma, T8877) in PBS at 37 °C for 10 min. After incubation, heart sections were fixed in 4% paraformaldehyde for 30 min and photographed. To assess the infarct size, *ImageJ* software (NIH) was utilized for measurement, where the TTC-negative area (pan) represented the infarcted myocardium, and the TTC-stained area appeared red. Myocardial infarct size was presented as a proportion of total left ventricular area expressed as a percentage.[61]

Masson's Trichrome Staining. For Masson's trichrome staining, paraffin-embedded heart slices were dewaxed and rehydrated using an ethanol gradient. After rinsing with distilled water, the sections were stained with Masson's trichrome following the manufacturer's protocol (HT15; Sigma-Aldrich). All images were captured at 4× magnification using a light microscope (Nikon Eclipse TE2000-S). The scar size was determined by calculating the total infarct circumference divided by the total LV circumference using *ImageJ* software.[62]

Wheat Germ Agglutinin (WGA) Staining. For the measurement of the cardiomyocyte cross-sectional area, heart sections were deparaffinized, rehydrated, and washed. After blocking with 5% BSA for 30 min, sections were incubated with Alexa Fluor 488 Conjugate WGA (5 g/mL, Invitrogen, W11261) for 1 h, followed by costaining with DAPI. To quantify cell size, each of six independent hearts was imaged with three different fields of view in both the border peri-infarct zone and the remote zone and photographed at a magnification of 40×. *ImageJ* was utilized to measure the size of the round cardiomyocytes containing nuclei. Over 200 cells per heart were measured, and the average values were used for analysis.[63]

Hematoxylin and Eosin (HE) Staining. HE staining was carried out following standard procedures. Tissue sections from the heart, liver, kidneys, and lungs of the mice underwent deparaffinization, rehydration, and washing. Subsequently, the sections were incubated with HE. Images were captured at 200× magnification using a light microscope (Nikon Ni-E). To ensure an unbiased histopathologic assessment, a blinded evaluation was performed by three experienced pathologists from Anzhen Hospital (Beijing, China) using a comprehensive 12-point histologic scoring system.[64,65]

Tube Formation Assay. Tube formation assay was conducted as described in previous studies.[66] In summary, growth factor-reduced Matrigel (BD Biosciences, 354230) was plated in a 24-well plate (200 μL/well) after overnight thawing at 4 °C and polymerized for 1 h at 37 °C. HUVECs, sourced from the American Type Culture Collection (ATCC; Manassas, VA) were cultured in endothelial cell medium (ECM; ScienCell, #1001) containing 5% FBS, 1% EC Growth Supplement, and 1% penicillin/streptomycin solution. HUVECs transduced with CPE/pCXCL12 or CPC/pCXCL12 were seeded into Matrigel-coated wells (1×10^5 cells/well). After culturing for 8 h, the total number of capillary tube branches per field was observed and quantified by counting random fields per well under a microscope.

Adhesion Assay. HUVECs were seeded in a 24-well plate at a density of 1×10^5 cells per well and allowed to adhere overnight. Upon reaching confluence, HUVECs were transduced with CPE/siR-ICAM1 or CPC/siR-ICAM1 for 24 h. Bone marrow-derived macrophages (BMDMs) were stained with 2 μM Calcein AM (Invitrogen, C3100) for 1 h and then added to HUVECs at a density of 5×10^5 cells/well. Following a one h incubation, nonadherent BMDMs were washed with PBS. Subsequently, 1 mL of PBS was added to each well, and the fluorescence intensity of the labeled BMDMs was measured using an ImageXpress Micro XLS (Molecular Devices) at excitation and emission wavelengths of 485 and 538 nm, respectively.[67]

Flow Cytometry. One day post-MI, hearts were perfused with prechilled saline. The left ventricle was then isolated, finely minced with scissors, and digested in Hank's Balanced Salt Solution (HBSS; Gibco, 14170112) containing collagenase II (200 U/mL; Thermo-Fisher, 17101015) and Dispase II (1 U/mL; Roche, 04942078001) at 37 °C for 30 min. After digestion, the mixture was filtered through a 40 μm filter to generate a single-cell suspension. The cells were incubated with fluorescently conjugated antibodies, including PerCP-Cy5.5-CD45 (BD, 550994), APC-Cy7-CD11b (BD, 557657), PE-F4/80 (BD, 565410), PE-CF594-Ly6G (BD, 562700), and BV605-Ly6C (BD, 563011) at 4 °C in the dark for 40 min. Subsequently, the cells were washed with staining buffer (PBS containing 0.04% BSA) and analyzed using a BD LSRFortessa flow cytometer following the manufacturer's protocol.[68]

Coronary Vascular Perfusion and Imaging. Mice were anesthetized with isoflurane and retrogradely cannulated via the

descending thoracic aorta. To visualize coronary arterial stress, the vasculature was cleared by perfusion with saline containing heparin sodium salt (25 U/mL). Following this, vessels were fixed by being perfused with 4% paraformaldehyde (PFA). Yellow Microfil (8:1:1 latex:diluent:curing agent; Flow Tech, Carver, MA, U.S.A.) was then perfused throughout the vasculature. After Microfil polymerization and overnight fixation with 4% PFA, hearts were imaged using microcomputed tomography (micro-CT) on a Siemens Inveon PET/CT scanner, and 3D reconstruction of the perfused vasculature was performed. Regions of interest (ROI) were delineated to identify the infarct or equivalent areas in sham-ligated animals. Mean ROI values were extracted for the analysis of vessel coverage in the infarction zone using Inveon Research Workplace software.[69]

RNA Sequencing. Three days post-MI or sham operation, LV tissue was collected, and RNA was extracted using TRIzol reagent (Invitrogen, 15596018). For RNA sample preparation, 1 μg of RNA per sample was used as the input material. Sequencing libraries were then constructed using the NEBNext UltraTM RNA Library Prep Kit for Illumina (NEB, U.S.A.), and the resultant libraries were sequenced on an Illumina NovaSeq6000 platform. Following quality control, featureCounts v1.5.0-p3 was employed to tally the read numbers mapped to each gene. The Fragments Per Kilobase of transcript per Million mapped reads (FPKM) for each gene was computed based on the gene's length and the mapped read count. Differentially expressed genes (DEGs) were pinpointed utilizing the DESeq2 package (|Log2 fold change | ≥ 0.5, $P < 0.05$). Gene Set Enrichment Analysis (GSEA) was carried out utilizing the KEGG database, and the resultant GSEA data were scrutinized and presented in an enrichment plot using the R package clusterProfiler. A significance threshold of $P < 0.05$ was applied.

Statistical Analysis. Data are presented as the mean ± standard error of the mean, and statistical analyses were conducted using GraphPad Prism version 8 (GraphPad Software, CA, U.S.A.). Normality was assessed using the Shapiro-Wilk test. If the data conformed to a normal distribution, an unpaired two-tailed Student's t-test was used to compare differences between two independent groups. For comparisons involving multiple groups, a one-way (one variable) analysis of variance (ANOVA) was performed, followed by Tukey's posthoc multiple comparison test. In cases where the data distribution deviated from normality, the Mann–Whitney U test was utilized for comparing two groups, and the Kruskal–Wallis test, followed by Dunn's multiple comparison test, was used for posthoc comparisons in the context of multiple groups. Across all analyses, $P < 0.05$ was considered statistically significant.

ASSOCIATED CONTENT

Ⓢℹ Supporting Information

The Supporting Information is available free of charge at https://pubs.acs.org/doi/10.1021/acsnano.3c11661.

> The stimulated systems of different complexes; ^{1}H NMR spectra of CHO-Br, CHO-PGMA, CHO-PGEA (CPE), CHO-PGEA/ED, and CHO-PGEA/ED-CRPPR (CPC); The amount of grafted targeting peptide was calculated by fluorescent intensity; Protein adsorption of all the complexes; Particle size stabilities of all the complexes; Images of red blood cells (RBCs) treated with PBS, water, PEI, CPE, and CPC; Cell type specificity of ICAM1 and CXCL12 in the heart; Biosafety of administration with CPC/siR-ICAM1+CPC/pCXCL12 complex; PDI values of all the complexes; Echocardiographic analysis in the mice administered with each complex 14 days post-MI (PDF)

AUTHOR INFORMATION

Corresponding Authors

Yulin Li − *Beijing Anzhen Hospital of Capital Medical University and Beijing Institute of Heart Lung and Blood Vessel Diseases, Beijing 100029, China;* Email: lyllyl_1111@163.com

Fu-Jian Xu − *State Key Laboratory of Chemical Resource Engineering, Key Lab of Biomedical Materials of Natural Macromolecules (Beijing University of Chemical Technology, Ministry of Education) and Laboratory of Biomedical Materials, College of Materials Science and Engineering, Beijing University of Chemical Technology, Beijing 100029, China;* ⓞ orcid.org/0000-0002-1838-8811; Email: xufj@mail.buct.edu.cn

Authors

Yihui Shao − *Beijing Anzhen Hospital of Capital Medical University and Beijing Institute of Heart Lung and Blood Vessel Diseases, Beijing 100029, China*

Chen Xu − *State Key Laboratory of Chemical Resource Engineering, Key Lab of Biomedical Materials of Natural Macromolecules (Beijing University of Chemical Technology, Ministry of Education) and Laboratory of Biomedical Materials, College of Materials Science and Engineering, Beijing University of Chemical Technology, Beijing 100029, China*

Shuolin Zhu − *Beijing Anzhen Hospital of Capital Medical University and Beijing Institute of Heart Lung and Blood Vessel Diseases, Beijing 100029, China*

Jianing Wu − *Beijing Anzhen Hospital of Capital Medical University and Beijing Institute of Heart Lung and Blood Vessel Diseases, Beijing 100029, China*

Canghao Sun − *Beijing Anzhen Hospital of Capital Medical University and Beijing Institute of Heart Lung and Blood Vessel Diseases, Beijing 100029, China*

Shan Huang − *Beijing Anzhen Hospital of Capital Medical University and Beijing Institute of Heart Lung and Blood Vessel Diseases, Beijing 100029, China*

Guoqi Li − *Beijing Anzhen Hospital of Capital Medical University and Beijing Institute of Heart Lung and Blood Vessel Diseases, Beijing 100029, China*

Weijie Yang − *State Key Laboratory of Chemical Resource Engineering, Key Lab of Biomedical Materials of Natural Macromolecules (Beijing University of Chemical Technology, Ministry of Education) and Laboratory of Biomedical Materials, College of Materials Science and Engineering, Beijing University of Chemical Technology, Beijing 100029, China*

Ting Zhang − *State Key Laboratory of Chemical Resource Engineering, Key Lab of Biomedical Materials of Natural Macromolecules (Beijing University of Chemical Technology, Ministry of Education) and Laboratory of Biomedical Materials, College of Materials Science and Engineering, Beijing University of Chemical Technology, Beijing 100029, China*

Xin-Liang Ma − *Department of Emergency Medicine, Thomas Jefferson University, Philadelphia, Pennsylvania 19107, United States*

Jie Du − *Beijing Anzhen Hospital of Capital Medical University and Beijing Institute of Heart Lung and Blood Vessel Diseases, Beijing 100029, China*

Ping Li − *Beijing Anzhen Hospital of Capital Medical University and Beijing Institute of Heart Lung and Blood Vessel Diseases, Beijing 100029, China*

Complete contact information is available at:
https://pubs.acs.org/10.1021/acsnano.3c11661

Author Contributions

[#]These authors contributed equally to this work (Y.S. and C.X.). Y.L., Y.S., and C.X. designed the experiments, conducted the experiments, analyzed the data, and wrote the manuscript. J.D., X-L.M., and F.-J.X. reviewed/edited the manuscript. S.Z. and C.S. assisted with animal experiments, surgeries, and histological analysis. J.W. and S.H. assisted with *in vitro* studies. W.Y. and T.Z. assisted with nanoparticles preparation. P.L. and J.W. performed the clinical study and interpreted the data.

Notes

The authors declare no competing financial interest.

REFERENCES

(1) Bergmark, B. A.; Mathenge, N.; Merlini, P. A.; Lawrence-Wright, M. B.; Giugliano, R. P. Acute coronary syndromes. *Lancet* **2022**, *399* (10332), 1347−1358.

(2) Clemente-Moragon, A.; Gomez, M.; Villena-Gutierrez, R.; Lalama, D. V.; Garcia-Prieto, J.; Martinez, F.; Sanchez-Cabo, F.; Fuster, V.; Oliver, E.; Ibanez, B. Metoprolol exerts a non-class effect against ischaemia-reperfusion injury by abrogating exacerbated inflammation. *European heart journal* **2020**, *41* (46), 4425−4440.

(3) Wang, Y.; Dembowsky, K.; Chevalier, E.; Stuve, P.; Korf-Klingebiel, M.; Lochner, M.; Napp, L. C.; Frank, H.; Brinkmann, E.; Kanwischer, A.; et al. C-X-C Motif Chemokine Receptor 4 Blockade Promotes Tissue Repair After Myocardial Infarction by Enhancing Regulatory T Cell Mobilization and Immune-Regulatory Function. *Circulation* **2019**, *139* (15), 1798−1812.

(4) Wang, Z.; Qiu, Z.; Hua, S.; Yang, W.; Chen, Y.; Huang, F.; Fan, Y.; Tong, L.; Xu, T.; Tong, X.; et al. Nuclear Tkt promotes ischemic heart failure via the cleaved Parp1/Aif axis. *Basic Research in Cardiology* **2022**, *117* (1), 18.

(5) Seiler, C.; Stoller, M.; Pitt, B.; Meier, P. The human coronary collateral circulation: development and clinical importance. *European heart journal* **2013**, *34* (34), 2674−2682.

(6) Heusch, G. Myocardial ischaemia-reperfusion injury and cardioprotection in perspective. *Nature Reviews Cardiology* **2020**, *17* (12), 773−789.

(7) Keller, T. C. S. t.; Lim, L.; Shewale, S. V.; McDaid, K.; Marti-Pamies, I.; Tang, A. T.; Wittig, C.; Guerrero, A. A.; Sterling, S.; Leu, N. A.; et al. Genetic blockade of lymphangiogenesis does not impair cardiac function after myocardial infarction. *J. Clin. Invest.* **2021**, *131* (20), No. e147070.

(8) Bai, P. Y.; Chen, S. Q.; Jia, D. L.; Pan, L. H.; Liu, C. B.; Liu, J.; Luo, W.; Yang, Y.; Sun, M. Y.; Wan, N. F.; et al. Environmental eustress improves postinfarction cardiac repair via enhancing cardiac macrophage survival. *Science Advances* **2022**, *8* (17), No. eabm3436.

(9) Forte, E.; Perkins, B.; Sintou, A.; Kalkat, H. S.; Papanikolaou, A.; Jenkins, C.; Alsubaie, M.; Chowdhury, R. A.; Duffy, T. M.; Skelly, D. A.; et al. Cross-Priming Dendritic Cells Exacerbate Immunopathology After Ischemic Tissue Damage in the Heart. *Circulation* **2021**, *143* (8), 821−836.

(10) Frantz, S.; Hundertmark, M. J.; Schulz-Menger, J.; Bengel, F. M.; Bauersachs, J. Left ventricular remodelling post-myocardial infarction: pathophysiology, imaging, and novel therapies. *European heart journal* **2022**, *43* (27), 2549−2561.

(11) Liu, R. R.; Li, J.; Gong, J. Y.; Kuang, F.; Liu, J. Y.; Zhang, Y. S.; Ma, Q. L.; Song, C. J.; Truax, A. D.; Gao, F.; et al. MicroRNA-141 regulates the expression level of ICAM-1 on endothelium to decrease myocardial ischemia-reperfusion injury. *American journal of physiology. Heart and circulatory physiology* **2015**, *309* (8), H1303−1313.

(12) Sager, H. B.; Dutta, P.; Dahlman, J. E.; Hulsmans, M.; Courties, G.; Sun, Y.; Heidt, T.; Vinegoni, C.; Borodovsky, A.; Fitzgerald, K.; et al. RNAi targeting multiple cell adhesion molecules reduces immune cell recruitment and vascular inflammation after myocardial infarction. *Sci. Transl Med.* **2016**, *8* (342), No. 342ra380.

(13) Placek, K.; Schultze, J. L.; Aschenbrenner, A. C. Epigenetic reprogramming of immune cells in injury, repair, and resolution. *J. Clin. Invest.* **2019**, *129* (8), 2994−3005.

(14) Marin-Juez, R.; El-Sammak, H.; Helker, C. S. M.; Kamezaki, A.; Mullapuli, S. T.; Bibli, S. I.; Foglia, M. J.; Fleming, I.; Poss, K. D.; Stainier, D. Y. R. Coronary Revascularization During Heart Regeneration Is Regulated by Epicardial and Endocardial Cues and Forms a Scaffold for Cardiomyocyte Repopulation. *Dev Cell* **2019**, *51* (4), 503−515.

(15) Lv, Y.; Kim, K.; Sheng, Y.; Cho, J.; Qian, Z.; Zhao, Y. Y.; Hu, G.; Pan, D.; Malik, A. B.; Hu, G. YAP Controls Endothelial Activation and Vascular Inflammation Through TRAF6. *Circulation research* **2018**, *123* (1), 43−56.

(16) MacArthur, J. W.; Cohen, J. E.; McGarvey, J. R.; Shudo, Y.; Patel, J. B.; Trubelja, A.; Fairman, A. S.; Edwards, B. B.; Hung, G.; Hiesinger, W.; et al. Preclinical Evaluation of the Engineered Stem Cell Chemokine Stromal Cell−Derived Factor 1α Analog in a Translational Ovine Myocardial Infarction Model. *Circulation research* **2014**, *114* (4), 650−659.

(17) Anderluh, M.; Kocic, G.; Tomovic, K.; Kocic, R.; Deljanin-Ilic, M.; Smelcerovic, A. Cross-talk between the dipeptidyl peptidase-4 and stromal cell-derived factor-1 in stem cell homing and myocardial repair: Potential impact of dipeptidyl peptidase-4 inhibitors. *Pharmacology & therapeutics* **2016**, *167*, 100−107.

(18) Das, S.; Goldstone, A. B.; Wang, H.; Farry, J.; D'Amato, G.; Paulsen, M. J.; Eskandari, A.; Hironaka, C. E.; Phansalkar, R.; Sharma, B.; et al. A Unique Collateral Artery Development Program Promotes Neonatal Heart Regeneration. *Cell* **2019**, *176* (5), 1128−1142.

(19) Jiang, X.; Shao, M.; Liu, X.; Liu, X.; Zhang, X.; Wang, Y.; Yin, K.; Wang, S.; Hu, Y.; Jose, P. A.; et al. Reversible Treatment of Pressure Overload-Induced Left Ventricular Hypertrophy through Drd5 Nucleic Acid Delivery Mediated by Functional Polyaminoglycoside. *Advanced Science* **2021**, *8* (5), No. 2003706.

(20) Park, J. S.; Yang, H. N.; Yi, S. W.; Kim, J. H.; Park, K. H. Neoangiogenesis of human mesenchymal stem cells transfected with peptide-loaded and gene-coated PLGA nanoparticles. *Biomaterials* **2016**, *76*, 226−237.

(21) Kim, D.; Hong, J.; Moon, H. H.; Nam, H. Y.; Mok, H.; Jeong, J. H.; Kim, S. W.; Choi, D.; Kim, S. H. Anti-apoptotic cardioprotective effects of SHP-1 gene silencing against ischemia-reperfusion injury: use of deoxycholic acid-modified low molecular weight polyethyleneimine as a cardiac siRNA-carrier. *Journal of controlled release: official journal of the Controlled Release Society* **2013**, *168* (2), 125−134.

(22) Zhi, Y.; Xu, C.; Sui, D.; Du, J.; Xu, F. J.; Li, Y. Effective Delivery of Hypertrophic miRNA Inhibitor by Cholesterol-Containing Nano-carriers for Preventing Pressure Overload Induced Cardiac Hypertrophy. *Advanced Science* **2019**, *6* (11), No. 1900023.

(23) Zhang, L.; Hoffman, J. A.; Ruoslahti, E. Molecular profiling of heart endothelial cells. *Circulation* **2005**, *112* (11), 1601−1611.

(24) Xu, J.; Lv, J.; Zhuang, Q.; Yang, Z.; Cao, Z.; Xu, L.; Pei, P.; Wang, C.; Wu, H.; Dong, Z.; et al. A general strategy towards personalized nanovaccines based on fluoropolymers for post-surgical cancer immunotherapy. *Nature Nanotechnol.* **2020**, *15* (12), 1043−1052.

(25) Patil, M. L.; Zhang, M.; Minko, T. Multifunctional triblock Nanocarrier (PAMAM-PEG-PLL) for the efficient intracellular siRNA delivery and gene silencing. *ACS Nano* **2011**, *5* (3), 1877−1887.

(26) Yan, J.; Liu, X.; Wu, F.; Ge, C.; Ye, H.; Chen, X.; Wei, Y.; Zhou, R.; Duan, S.; Zhu, R.; et al. Platelet Pharmacytes for the Hierarchical Amplification of Antitumor Immunity in Response to Self-Generated Immune Signals. *Advanced Materials* **2022**, *34* (23), No. e2109517.

(27) Xu, C.; Zhang, Y.; Xu, K.; Nie, J. J.; Yu, B.; Li, S.; Cheng, G.; Li, Y.; Du, J.; Xu, F. J. Multifunctional cationic nanosystems for nucleic acid therapy of thoracic aortic dissection. *Nat. Commun.* **2019**, *10* (1), 3184.

(28) Zhang, D.; Wang, G.; Yu, X.; Wei, T.; Farbiak, L.; Johnson, L. T.; Taylor, A. M.; Xu, J.; Hong, Y.; Zhu, H.; et al. Enhancing CRISPR/Cas gene editing through modulating cellular mechanical properties for cancer therapy. *Nature Nanotechnol.* **2022**, *17* (7), 777−787.

(29) Fukushima, S.; Coppen, S. R.; Varela-Carver, A.; Yamahara, K.; Sarathchandra, P.; Smolenski, R. T.; Yacoub, M. H.; Suzuki, K. A novel strategy for myocardial protection by combined antibody therapy inhibiting both P-selectin and intercellular adhesion molecule-1 via retrograde intracoronary route. *Circulation* **2006**, *114* (1 Suppl), I251−256.

(30) Goldstone, A. B.; Burnett, C. E.; Cohen, J. E.; Paulsen, M. J.; Eskandari, A.; Edwards, B. E.; Ingason, A. B.; Steele, A. N.; Patel, J. B.; MacArthur, J. W.; et al. SDF 1-alpha Attenuates Myocardial Injury Without Altering the Direct Contribution of Circulating Cells. *Journal of cardiovascular translational research* **2018**, *11* (4), 274−284.

(31) Ziff, O. J.; Bromage, D. I.; Yellon, D. M.; Davidson, S. M. Therapeutic strategies utilizing SDF-1alpha in ischaemic cardiomyopathy. *Cardiovascular research* **2018**, *114* (3), 358−367.

(32) Muhlstedt, S.; Ghadge, S. K.; Duchene, J.; Qadri, F.; Jarve, A.; Vilianovich, L.; Popova, E.; Pohlmann, A.; Niendorf, T.; Boye, P.; et al. Cardiomyocyte-derived CXCL12 is not involved in cardiogenesis but plays a crucial role in myocardial infarction. *Journal of molecular medicine* **2016**, *94* (9), 1005−1014.

(33) Li, Y.; Chen, X.; Jin, R.; Chen, L.; Dang, M.; Cao, H.; Dong, Y.; Cai, B.; Bai, G.; Gooding, J. J.; et al. Injectable hydrogel with MSNs/microRNA-21-5p delivery enables both immunomodification and enhanced angiogenesis for myocardial infarction therapy in pigs. *Science Advances* **2021**, *7* (9), No. eabd6740.

(34) Sun, Z.; Xie, Y.; Lee, R. J.; Chen, Y.; Jin, Q.; Lv, Q.; Wang, J.; Yang, Y.; Li, Y.; Cai, Y.; et al. Myocardium-targeted transplantation of PHD2 shRNA-modified bone mesenchymal stem cells through ultrasound-targeted microbubble destruction protects the heart from acute myocardial infarction. *Theranostics* **2020**, *10* (11), 4967−4982.

(35) Zbinden, A.; Layland, S. L.; Urbanczyk, M.; Carvajal Berrio, D. A.; Marzi, J.; Zauner, M.; Hammerschmidt, A.; Brauchle, E. M.; Sudrow, K.; Fink, S.; et al. Nidogen-1 Mitigates Ischemia and Promotes Tissue Survival and Regeneration. *Advanced Science* **2021**, *8* (4), No. 2002500.

(36) Lv, Q.; Ma, B.; Li, W.; Fu, G.; Wang, X.; Xiao, Y. Nanomaterials-Mediated Therapeutics and Diagnosis Strategies for Myocardial Infarction. *Front Chem.* **2022**, *10*, No. 943009.

(37) Kim, H.; Mun, D.; Kang, J. Y.; Lee, S. H.; Yun, N.; Joung, B. Improved cardiac-specific delivery of RAGE siRNA within small extracellular vesicles engineered to express intense cardiac targeting peptide attenuates myocarditis. *Molecular therapy. Nucleic acids* **2021**, *24*, 1024−1032.

(38) Zahid, M.; Feldman, K. S.; Garcia-Borrero, G.; Feinstein, T. N.; Pogodzinski, N.; Xu, X.; Yurko, R.; Czachowski, M.; Wu, Y. L.; Mason, N. S.; et al. Cardiac Targeting Peptide, a Novel Cardiac Vector: Studies in Bio-Distribution, Imaging Application, and Mechanism of Transduction. *Biomolecules* **2018**, *8* (4), 147.

(39) Parma, L.; Baganha, F.; Quax, P. H. A.; de Vries, M. R. Plaque angiogenesis and intraplaque hemorrhage in atherosclerosis. *European journal of pharmacology* **2017**, *816*, 107−115.

(40) Ballabh, P.; Xu, H.; Hu, F.; Braun, A.; Smith, K.; Rivera, A.; Lou, N.; Ungvari, Z.; Goldman, S. A.; Csiszar, A.; et al. Angiogenic inhibition reduces germinal matrix hemorrhage. *Nature medicine* **2007**, *13* (4), 477−485.

(41) Reed, G. W.; Rossi, J. E.; Cannon, C. P. Acute myocardial infarction. *Lancet* **2017**, *389* (10065), 197−210.

(42) Chen, Z. M.; Jiang, L. X.; Chen, Y. P.; Xie, J. X.; Pan, H. C.; Peto, R.; Collins, R.; Liu, L. S.; group, C. c.. Addition of clopidogrel to aspirin in 45,852 patients with acute myocardial infarction: randomised placebo-controlled trial. *Lancet* **2005**, *366* (9497), 1607−1621.

(43) Cheung, N.; Mitchell, P.; Wong, T. Y. Diabetic retinopathy. *Lancet* **2010**, *376* (9735), 124−136.

(44) Korpisalo, P.; Hytonen, J. P.; Laitinen, J. T.; Laidinen, S.; Parviainen, H.; Karvinen, H.; Siponen, J.; Marjomaki, V.; Vajanto, I.; Rissanen, T. T.; et al. Capillary enlargement, not sprouting angiogenesis, determines beneficial therapeutic effects and side effects of angiogenic gene therapy. *European heart journal* **2011**, *32* (13), 1664−1672.

(45) Passaro, F.; Testa, G.; Ambrosone, L.; Costagliola, C.; Tocchetti, C. G.; di Nezza, F.; Russo, M.; Pirozzi, F.; Abete, P.; Russo, T.; et al. Nanotechnology-Based Cardiac Targeting and Direct Cardiac Reprogramming: The Betrothed. *Stem Cells Int.* **2017**, *2017*, 1−12.

(46) Nguyen, M. M.; Carlini, A. S.; Chien, M. P.; Sonnenberg, S.; Luo, C.; Braden, R. L.; Osborn, K. G.; Li, Y.; Gianneschi, N. C.; Christman, K. L. Enzyme-Responsive Nanoparticles for Targeted Accumulation and Prolonged Retention in Heart Tissue after Myocardial Infarction. *Advanced materials* **2015**, *27* (37), 5547−5552.

(47) Lundy, D. J.; Chen, K. H.; Toh, E. K.; Hsieh, P. C. Distribution of Systemically Administered Nanoparticles Reveals a Size-Dependent Effect Immediately following Cardiac Ischaemia-Reperfusion Injury. *Sci. Rep.* **2016**, *6*, No. 25613.

(48) Zhao, X.; Luo, W.; Hu, J.; Zuo, L.; Wang, J.; Hu, R.; Wang, B.; Xu, L.; Li, J.; Wu, M.; et al. Cardiomyocyte-targeted and 17beta-estradiol-loaded acoustic nanoprobes as a theranostic platform for cardiac hypertrophy. *J. Nanobiotechnol.* **2018**, *16* (1), 36.

(49) Chen, J.; Yang, J.; Liu, R.; Qiao, C.; Lu, Z.; Shi, Y.; Fan, Z.; Zhang, Z.; Zhang, X. Dual-targeting Theranostic System with Mimicking Apoptosis to Promote Myocardial Infarction Repair via Modulation of Macrophages. *Theranostics* **2017**, *7* (17), 4149−4167.

(50) Abraham, M. J.; Murtola, T.; Schulz, R.; Páll, S.; Smith, J. C.; Hess, B.; Lindahl, E. GROMACS: High performance molecular simulations through multi-level parallelism from laptops to supercomputers. *SoftwareX* **2015**, *1−2*, 19−25.

(51) Lindorff-Larsen, K.; Piana, S.; Palmo, K.; Maragakis, P.; Klepeis, J. L.; Dror, R. O.; Shaw, D. E. Improved side-chain torsion potentials for the Amber ff99SB protein force field. *Proteins* **2010**, *78* (8), 1950−1958.

(52) Ziebarth, J. D.; Kennetz, D. R.; Walker, N. J.; Wang, Y. Structural Comparisons of PEI/DNA and PEI/siRNA Complexes Revealed with Molecular Dynamics Simulations. *J. Phys. Chem. B* **2017**, *121* (8), 1941−1952.

(53) Lu, T.; Chen, F. Multiwfn: a multifunctional wavefunction analyzer. *J. Comput. Chem.* **2012**, *33* (5), 580−592.

(54) Izadi, S.; Onufriev, A. V. Accuracy limit of rigid 3-point water models. *J. Chem. Phys.* **2016**, *145* (7), No. 074501.

(55) Essmann, U.; Perera, L.; Berkowitz, M. L.; Darden, T.; Lee, H.; Pedersen, L. G. A smooth particle mesh Ewald method. *J. Chem. Phys.* **1995**, *103* (19), 8577−8593.

(56) Li, Y.; Chen, B.; Yang, X.; Zhang, C.; Jiao, Y.; Li, P.; Liu, Y.; Li, Z.; Qiao, B.; Bond Lau, W.; et al. S100a8/a9 Signaling Causes Mitochondrial Dysfunction and Cardiomyocyte Death in Response to Ischemic/Reperfusion Injury. *Circulation* **2019**, *140* (9), 751−764.

(57) Sun, J. Y.; Du, L. J.; Shi, X. R.; Zhang, Y. Y.; Liu, Y.; Wang, Y. L.; Chen, B. Y.; Liu, T.; Zhu, H.; Liu, Y.; et al. An IL-6/STAT3/MR/

FGF21 axis mediates heart-liver cross-talk after myocardial infarction. *Science Advances* **2023**, *9* (14), No. eade4110.

(58) Li, Y.; Li, Z.; Zhang, C.; Li, P.; Wu, Y.; Wang, C.; Bond Lau, W.; Ma, X. L.; Du, J. Cardiac Fibroblast-Specific Activating Transcription Factor 3 Protects Against Heart Failure by Suppressing MAP2K3-p38 Signaling. *Circulation* **2017**, *135* (21), 2041−2057.

(59) Pan, X.; Shao, Y.; Wu, F.; Wang, Y.; Xiong, R.; Zheng, J.; Tian, H.; Wang, B.; Wang, Y.; Zhang, Y.; et al. FGF21 Prevents Angiotensin II-Induced Hypertension and Vascular Dysfunction by Activation of ACE2/Angiotensin-(1−7) Axis in Mice. *Cell metabolism* **2018**, *27* (6), 1323−1337.

(60) Lebek, S.; Chemello, F.; Caravia, X. M.; Tan, W.; Li, H.; Chen, K.; Xu, L.; Liu, N.; Bassel-Duby, R.; Olson, E. N. Ablation of CaMKIIdelta oxidation by CRISPR-Cas9 base editing as a therapy for cardiac disease. *Science* **2023**, *379* (6628), 179−185.

(61) Ponnalagu, D.; Hamilton, S.; Sanghvi, S.; Antelo, D.; Schwieterman, N.; Hansra, I.; Xu, X.; Gao, E.; Edwards, J. C.; Bansal, S. S.; et al. CLIC4 localizes to mitochondrial-associated membranes and mediates cardioprotection. *Science Advances* **2022**, *8* (42), No. eabo1244.

(62) Tani, H.; Sadahiro, T.; Yamada, Y.; Isomi, M.; Yamakawa, H.; Fujita, R.; Abe, Y.; Akiyama, T.; Nakano, K.; Kuze, Y.; et al. Direct Reprogramming Improves Cardiac Function and Reverses Fibrosis in Chronic Myocardial Infarction. *Circulation* **2023**, *147* (3), 223−238.

(63) Abouleisa, R. R. E.; Salama, A. B. M.; Ou, Q.; Tang, X. L.; Solanki, M.; Guo, Y.; Nong, Y.; McNally, L.; Lorkiewicz, P. K.; Kassem, K. M.; et al. Transient Cell Cycle Induction in Cardiomyocytes to Treat Subacute Ischemic Heart Failure. *Circulation* **2022**, *145* (17), 1339−1355.

(64) Fernandez, A. F.; Sebti, S.; Wei, Y.; Zou, Z.; Shi, M.; McMillan, K. L.; He, C.; Ting, T.; Liu, Y.; Chiang, W. C.; et al. Disruption of the beclin 1-BCL2 autophagy regulatory complex promotes longevity in mice. *Nature* **2018**, *558* (7708), 136−140.

(65) Chandrashekar, A.; Yu, J.; McMahan, K.; Jacob-Dolan, C.; Liu, J.; He, X.; Hope, D.; Anioke, T.; Barrett, J.; Chung, B.; et al. Vaccine protection against the SARS-CoV-2 Omicron variant in macaques. *Cell* **2022**, *185* (9), 1549−1555.

(66) Kan, X.; Wu, Y.; Ma, Y.; Zhang, C.; Li, P.; Wu, L.; Zhang, S.; Li, Y.; Du, J. Deficiency of IL-12p35 improves cardiac repair after myocardial infarction by promoting angiogenesis. *Cardiovascular research* **2016**, *109* (2), 249−259.

(67) Xu, K.; Saaoud, F.; Yu, S.; Drummer, C. t.; Shao, Y.; Sun, Y.; Lu, Y.; Sun, J.; Yu, J.; Jiang, X.; et al. Monocyte Adhesion Assays for Detecting Endothelial Cell Activation in Vascular Inflammation and Atherosclerosis. *Methods in molecular biology* **2022**, *2419*, 169−182.

(68) Sreejit, G.; Nooti, S. K.; Jaggers, R. M.; Athmanathan, B.; Ho Park, K.; Al-Sharea, A.; Johnson, J.; Dahdah, A.; Lee, M. K. S.; Ma, J.; et al. Retention of the NLRP3 Inflammasome-Primed Neutrophils in the Bone Marrow Is Essential for Myocardial Infarction-Induced Granulopoiesis. *Circulation* **2022**, *145* (1), 31−44.

(69) Munarin, F.; Kant, R. J.; Rupert, C. E.; Khoo, A.; Coulombe, K. L. K. Engineered human myocardium with local release of angiogenic proteins improves vascularization and cardiac function in injured rat hearts. *Biomaterials* **2020**, *251*, No. 120033.